

# 1 Vegetation and geochemical responses to Holocene rapid 2 climate change in Sierra Nevada (SE Iberia): The Laguna 3 Hondera record

4 Jose Manuel Mesa-Fernández<sup>1, 2</sup>, Gonzalo Jiménez-Moreno<sup>1</sup>, Marta Rodrigo-Gámiz<sup>2</sup>,  
5 Antonio García-Alix<sup>1,2</sup>, Francisco J. Jiménez-Espejo<sup>3</sup>, Francisca Martínez-Ruiz<sup>2</sup>, R. Scott  
6 Anderson<sup>4</sup>, Jon Camuera<sup>1</sup> and María J. Ramos-Román<sup>1</sup>

7 <sup>1</sup> Departamento de Estratigrafía y Paleontología, Universidad de Granada (UGR), Avda. Fuente Nueva s/n,  
8 18002, Granada, Spain

9 <sup>2</sup> Instituto Andaluz de Ciencias de la Tierra (IACT), CSIC-UGR, Avenida de las Palmeras 4, 18100,  
10 Armilla, Granada, Spain

11 <sup>3</sup> Department of Biogeochemistry (JAMSTEC), Yokosuka, Japan.

12 <sup>4</sup> School of Earth Sciences and Environmental Sustainability, Northern Arizona University, Flagstaff, AZ,  
13 USA.

14 *Correspondance to:* Jose Manuel Mesa-Fernández (jmesa@iact.ugr-csic.es)

## 15 **Abstract.**

16 High-altitude peat bogs and lacustrine records are very sensitive to climate changes and atmospheric dust  
17 input. Recent studies have shown a close relationship between regional climate aridity and enhanced  
18 eolian input to lake sediments. However, changes in regional-scale dust fluxes due to climate variability  
19 at short-scales and how alpine environments were impacted by climatic- and human-induced  
20 environmental changes are not completely understood.

21 Here we present a multi-proxy (palynological, geochemical and magnetic susceptibility) lake sediment  
22 record of climate variability in the Sierra Nevada (SE Iberian Peninsula) over the Holocene. Magnetic  
23 susceptibility and geochemical proxies obtained from the high mountain lake record of Laguna Hondera  
24 evidence humid conditions during the Early Holocene, while a trend towards more arid conditions is  
25 recognized since ~7000 cal yr BP, with enhanced Saharan eolian dust deposition until Present. This trend  
26 towards enhanced arid conditions was modulated by millennial-scale climate variability. Relative humid  
27 conditions occurred during the Iberian Roman Humid Period (2600-1450 cal yr BP) and predominantly  
28 arid conditions occurred during the Dark Ages and the Medieval Climate Anomaly (1450-650 cal yr BP).  
29 The Little Ice Age (650-150 cal yr BP) is characterized in the LH record by an increase in runoff and a  
30 minimum in eolian input. In addition, we further suggest that human impact in the area is noticed through  
31 the record of *Olea* cultivation, *Pinus* reforestation and Pb pollution during the Industrial Period (150 cal yr  
32 BP-Present). Furthermore, we estimated that the correlation between Zr and Ca concentrations stands for  
33 Saharan dust input to the Sierra Nevada lake records. These assumptions support that present-day  
34 biochemical observations, pointing to eolian input as the main inorganic nutrient source for oligotrophic  
35 mountain lakes, are comparable to the past record of eolian supply to these high-altitude lakes.

## 36 **1. Introduction**

37 The southern Iberian Peninsula has been the location for a number of recent studies detailing past vegetation  
38 and former climate of the region (Carrión et al., 2001, 2003, 2007, 2010; Carrión, 2002; Combourieu  
39 Nebout et al., 2009; Jiménez-Espejo et al., 2008; Martín-Puertas et al., 2008, 2010; Fletcher et al., 2010;

40 Nieto-Moreno et al., 2011, 2015; Rodrigo-Gámiz et al., 2011; Moreno et al., 2012 Jiménez-Moreno et al.,  
41 2015). Some of these studies have also documented that the western Mediterranean area has been very  
42 sensitive to short-term climatic fluctuations throughout the Holocene (e.g., Fletcher and Sánchez-Goñi,  
43 2008; Combourieu Nebout et al., 2009; Fletcher et al., 2010; Jiménez-Moreno et al., 2013). However, a  
44 subset of recent studies have attempted to determine how Mediterranean alpine environments have been  
45 affected by Holocene climate change through the study of sedimentary records from high elevation  
46 wetlands in the Sierra Nevada (Anderson et al., 2011; García-Alix et al., 2012, 2013; Jiménez-Moreno and  
47 Anderson, 2012; Jiménez-Moreno et al., 2013; Jiménez-Espejo et al., 2014; Ramos-Román et al., 2016;  
48 García-Alix et al., 2017). These alpine lake and bog records show minimal anthropic influence because  
49 they are usually elevational higher than major regional Late Holocene human landscape modification. This  
50 allows for a potentially clearer climatic signal to be determined from these sites. Even though human impact  
51 is less important at high-elevations, the impacts of human activities has also been reconstructed from these  
52 Late Holocene sedimentary records (Anderson et al., 2011; García-Alix et al., 2012, 2013; 2017, 2018).  
53 Several studies have highlighted the role of atmospheric mineral dust deposition in marine (Pulido-Villena  
54 et al., 2008a) and terrestrial (Morales-Baquero et al., 1999; Ballantyne et al., 2011) ecosystem fertilization  
55 through major micronutrients supply. Similar results have been described in the Sierra Nevada alpine lakes,  
56 where Saharan dust is especially important in conditioning plankton communities from oligotrophic lakes  
57 (Morales-Baquero et al., 2006a, 2006b; Mladenov et al., 2008; Pulido-Villena et al., 2008b; Reche et al.,  
58 2009). Although this eolian signal has been occasionally recorded in the sedimentary sequences from the  
59 Sierra Nevada lakes (Jimenez-Espejo et al., 2014; García-Alix et al., 2017), the record of inorganic nutrients  
60 in Saharan dust input in past lake geochemistry has remained elusive. This study investigates a multiproxy  
61 sediment core record from Laguna Hondera (LH), located in the Sierra Nevada range with two main goals:  
62 (1) identifying and characterizing climatic variability during the Holocene, focusing on vegetation changes,  
63 eolian input and runoff sediments variations; and (2) understanding the Saharan dust influence in past lake  
64 sedimentation and geochemistry.

## 65 **2. Study Area**

66 Sierra Nevada is the highest mountain range in the southern Iberian Peninsula. Bedrock of the high  
67 elevations of the Sierra Nevada is mostly composed of metamorphic rocks, principally mica schists  
68 (Castillo Martín, 2009). During the late Pleistocene, the Sierra Nevada was one of the southernmost  
69 mountains to support alpine glaciers and its last advance was recorded during the Little Ice Age (LIA;  
70 Palma et al., 2017; Oliva et al., 2018). Subsequently to the melting of ice at the end of the Last Glacial  
71 Maximum, wetlands and small lakes formed in the glacial cirque basins, which occur between 2451 and  
72 3227 masl (Schulte, 2002; Castillo Martín, 2009; Palma et al., 2017). Several alpine wetland and lakes have  
73 been studied in this area during the last few years as shown in Figure 1.

### 74 **2.1. Regional Climate and Vegetation**

75 Mediterranean climate characterises southern Iberia, with a marked seasonal variation between warm and  
76 dry summers and cool and humid winters (e.g. Lionello et al., 2006). Overprinting this general climate is  
77 the influence of the North Atlantic Oscillation (NAO) (Trigo et al., 2004; Trouet et al., 2009). Southern

78 Iberia is also characterized by strong altitudinal contrasts, which in turn control the precipitation patterns,  
79 with mean annual values ranging from  $<400 \text{ mm yr}^{-1}$  to  $>1400 \text{ mm yr}^{-1}$  in the southeast desert lowlands  
80 and the southwest highland, respectively (Jiménez-Moreno et al., 2013 and references therein).  
81 As with most mountainous regions, species and species groupings in the Sierra Nevada are distributed with  
82 respect to elevation, depending on the temperature and rainfall gradients (e.g., El Aallali et al., 1998; Valle,  
83 2003). Above 2800 masl the oromediterranean flora occurs as tundra-like open grassland. The  
84 oromediterranean belt (1900-2800 masl) mostly includes dwarf *Juniperus* (juniper), xerophytic shrublands  
85 and pasturelands and *Pinus sylvestris* and *P. nigra*. The supramediterranean belt (~1400-1900 masl) is  
86 characterized by mixed deciduous and evergreen forest species (i.e., evergreen and deciduous *Quercus*,  
87 with *Pinus spp.* and others). Mesomediterranean vegetation (600-1400 masl) includes sclerophyllous  
88 shrublands and evergreen *Quercus* woodlands. The natural vegetation has been strongly altered by human  
89 activities and cultivation in the last centuries, increasing significantly the abundance of *Olea* (olive), due to  
90 cultivation at lower altitudes (Anderson et al., 2011, and references therein), and *Pinus* due to reforestation  
91 primarily at higher elevations (Valbuena-Carabaña, 2010).

## 92 **2.2. Laguna Hondera**

93 Laguna Hondera (hereafter LH; 2899 masl; 37°02.88'N, 3°17.66'W, lake surface: 0.0053 km<sup>2</sup>; maximum  
94 depth: 0.8 m; Morales-Baquero et al., 1999; Fig. 1) is a small and shallow lake located at the lowest  
95 elevation of a set of lakes locally named Cañada de Siete Lagunas, a glacial valley between two of the  
96 highest peaks of the mountain range in the Iberian Peninsula: Alcazaba (3366 masl) and Mulhacén (3479  
97 masl). LH has a large catchment area of 1.546 km<sup>2</sup>, which is much larger than previously studied sites in  
98 the region (Laguna de Río Seco, LdRS, 0.099 km<sup>2</sup>; Borreguil de la Caldera, BdlC, 0.62 km<sup>2</sup>; Morales-  
99 Baquero et al., 1999; Ramos-Román et al., 2016; Fig 1 for locations). The lake was reduced to a little pond  
100 in the deepest area of the basin when cored in September 2012, with a maximum depth of only a few  
101 centimetres.

102 LH presently occurs in the oromediterranean vegetation belt (2800 masl) (El Aallali et al., 1998; Valle  
103 et al., 2003). The bedrock in the LH basin consists in Paleozoic and Precambrian mica schist with disthene  
104 and staurolite of the lower part of the Caldera Formation (Díaz de Federico et al., 1980).

## 105 **3. Methods**

### 106 **3.1. Core sampling, lithology and chronology**

107 Six sediment cores were recovered from LH with a Livingstone piston corer in September 2012. LH 12-03  
108 (83 cm) was selected for a multi-proxy study because it was the longest core. Cores were wrapped with tin  
109 foil and plastic film and transported to Universidad de Granada, where they were stored at 4°C.

110 Core LH 12-03 was split longitudinally and the sediments were described. Magnetic susceptibility was  
111 measured every 0.5 cm with a Bartington MS2E meter in SI units ( $\times 10^{-4}$ ) (Fig. 2). The sediment cores were  
112 subsampled every 1 cm for several analyses, including pollen and geochemistry.

113 The age model was built using seven AMS radiocarbon dates from vegetal remains (Table 1; Fig. 2) by  
114 means of Clam software (Blaauw, 2010; version 2.2), which used the IntCal13 curve for radiocarbon age

115 calibration (Reimer et al., 2013). A smooth spline approach was chosen (Fig. 2). The sediment accumulation  
116 rate (SAR) was calculated with the average rate from the Clam smooth spline output (Fig. 2).

### 117 **3.2. Pollen**

118 Pollen analysis was performed on 1 cm<sup>3</sup> of sample collected at regular 1 cm interval throughout the first 62  
119 cm of the core. Older sediments (from 62 to 82 cm depth) were barren in pollen, and only one interval at  
120 73 cm could be studied (Fig. 2). Pollen extraction included HCl and HF treatment, sieving, and the addition  
121 of Lycopodium spores for calculation of pollen concentration (modified from Faegri and Iversen, 1989).  
122 Sieving was done using a 10 µm nylon sieve. The resulting pollen residue was suspended in glycerine and  
123 mounted on microscope slides. Slides were analysed at 400x magnification counting a minimum of 300  
124 pollen grains, not including the local aquatic species Cyperaceae, Ranunculaceae and *Typha*. An overview  
125 of pollen taxa with abundances >1% for core LH 12-03 is plotted using the Tilia software (Grimm, 1993)  
126 in Figure 3. The pollen zonation was delimited visually by a cluster analysis constrained by age of taxa  
127 abundance >1% using CONISS software (Grimm, 1987) (Fig. 3). *Olea* was differentiated from others  
128 Oleaceae, such as *Phillyrea*, based on the thicker intine and higher size of reticulum in polar vision (Beug,  
129 2004).

### 130 **3.3. Geochemical analyses**

131 X-ray fluorescence (XRF) Avaatech core scanner®, located at the University of Barcelona, was used to  
132 measure light and heavy elements in the LH 12-03 core. An X-ray current of 650 µA, a 10 second count  
133 time and 10 kV X-ray voltage was used for measuring light elements, whereas 1700 µA X-ray current, 35  
134 second count time and 30 kV X-ray voltage was used for heavy elements. Sampling interval for these  
135 analyses was every 0.5 cm. For our study only three elements (K, Ca and Ti) have been considered with  
136 enough counts to be representative.

137 Inductively coupled plasma-optical emission spectrometry (ICP-OES; Perkin-Elmer optima 8300) was  
138 used for major element analysis on discrete samples every 2 cm. Prior to analysis, the samples were dried  
139 in an oven and digested with HNO<sub>3</sub> and HF. Blanks and international standards were used for quality  
140 control, the analytical accuracy was higher than ± 2.79% and 1.89% for 50 ppm elemental concentrations  
141 of Al and Ca, respectively, and better than ± 0.44% for 5 ppm elemental concentrations of K.

142 Trace element analysis was performed with an inductively coupled plasma mass spectrometry (ICP-MS;  
143 Perkin Elmer Sciex Elan 5000). Samples were measured in triplicate through spectrometry using Re and  
144 Rh as internal standards. The instrumental error is 2% for elemental concentrations of 50 ppm (Bea, 1996).  
145 Both ICP-OES and ICP-MS analyses were performed at the Centre for Scientific Instrumentation (CIC),  
146 University of Granada, Spain.

### 147 **3.4. Mineralogical analyses**

148 Morphological and compositional analyses were performed using scanning electron microscopy (SEM)  
149 with an AURIGA model microscope (Carl Zeiss SMT) coupled with energy-dispersive X-ray microanalysis  
150 (EDX) and Electron Backscatter Diffraction (EBSD) mode, also at the CIC (University of Granada, Spain).  
151 Mineral grains were analysed to determine provenance, in particular those from eolian origin.

152 **3.5 Statistical Analysis**

153 R-mode principal components analysis (PCA) was run on the geochemical dataset using the PAST software  
154 (Hammer et al., 2001). PCA identifies hypothetical variables (components) accounting for as much as  
155 possible of the variance in multivariate data (Davis, 1986; Harper, 1999). The elements used in the PCA  
156 were standardized by subtracting the mean and dividing by the standard deviation (Davis, 1986). Pb was  
157 not included in the PCA analysis due to its anthropogenic origin from mining and industrial pollution during  
158 the latest Holocene in this area (García-Alix et al., 2013).

159 **4. Results**

160 **4.1. Lithology and magnetic susceptibility**

161 The LH 12-03 sediment core consists primarily of peat in the upper ~60 cm, with mostly sand and clay  
162 layers below (Fig. 2). Positive MS peaks coincide with the grey clay intervals between 58 and 72 cm. Peat  
163 intervals coincide with relatively low MS values. For example, a minimum in MS occurs at 36-48 cm depth,  
164 related with a peaty interval with root remains. Near the bottom of the core, between 76 and 80 cm, a sandy  
165 oxidized interval occurs.

166 **4.2. Chronology and sedimentation rate**

167 The age model of LH 12-03 documents that the record spans the last 10800 cal yr BP (Table 1; Fig. 2).  
168 Sediment accumulation rates (SAR) were calculated using the average rate from the Clam smooth spline  
169 output (Fig. 2). The SAR below ~39 cm is very constant, varying between 0.049 and 0.061 mm yr<sup>-1</sup>. The  
170 SAR increases exponentially to 0.098 mm yr<sup>-1</sup> at 22 cm, 0.167 mm yr<sup>-1</sup> at ~9 cm and 0.357 mm yr<sup>-1</sup> at the  
171 core top. Accordingly with the model age and the SAR, resolution of pollen analysis varies between ~40  
172 years per sample in the top of the core and ~120 years per sample in the lower part. The resolution of the  
173 geochemical analysis on discrete samples changes between 100 and 400 years per sample, but the  
174 geochemical XRF core scanning resolution ranges between 15 and 100 years per sample, providing higher  
175 resolution than geochemical data on discrete sample. The MS analyses resolution varies between 15 and  
176 100 years per sample.

177 **4.3. Pollen**

178 Fifty distinct pollen taxa were recognized, but only those with abundance higher than 1% are included in  
179 the pollen diagram (Fig. 3). Four pollen zones for the LH 12-03 record are identified, using variation in  
180 pollen species plotted in Figure 3 and a cluster analysis run through the CONISS software (Grimm, 1987).  
181 Zone LH-1 (core bottom-2600 cal yr BP) is subdivided in two subzones. Subzone LH-1A (bottom-4000 cal  
182 yr BP) is defined by the alternation between Arboreal Pollen (AP) and herbs. AP is composed primarily of  
183 *Pinus*, but also *Quercus*. During the interval from ~9500 to ~7000 cal yr, BP only three samples were  
184 analysed, due to the low preservation of pollen in this interval. Pollen in this period is dominated by an  
185 alternation between Asteraceae (3-60%) and *Pinus* (5-90%) (Fig. 3). The highest occurrence of Onagraceae  
186 (~10%) is identified in this subzone, and Caryophyllaceae reach high values (~10%) as well. Only minor  
187 amounts of graminoids (Poaceae and Cyperaceae) occur during this period.

188 Between ~7000 to ~4000, *Pinus* pollen decreases from 90 % to ~55%, with a minimum (~30%) at 5000 cal  
189 yr BP. *Quercus* increase from ~2% to ~10%. The highest percentages of *Betula* (~5%) in the record occurs  
190 at this time. Asteraceae pollen decreases (~5-30%), but Poaceae increase from <5% at the opening of the  
191 subzone to >25%. Cyperaceae occur in high percentages (15%).

192 The subzone LH-1B (~ 4000-2600 cal yr BP) is defined primarily by a great increase in Poaceae pollen (to  
193 ~60%) (Fig. 3). Other important herbs and shrubs include Asteraceae (5-15%) and Caryophyllaceae (~5%).  
194 Other pollen types that increase for the first time in this zone include Ericaceae (~3%), *Artemisia* (~3%)  
195 and Ranunculaceae (~2-6%). *Pinus* (~3-25%) and Cyperaceae (0-14%) record a minimum in this zone, and  
196 Onagraceae disappear altogether (Fig. 3).

197 Zone LH-2 (~ 2600-1450 cal yr BP) pollen assemblages show high variability. *Pinus* pollen variates  
198 between ~80% to ~3% from the onset to the end of the zone. Aquatic pollen such as Cyperaceae (~15%)  
199 increases. On the other hand, an increase in herbs such as Asteraceae (~5-70%) occurs along the zone,  
200 Poaceae pollen variates between ~7 and 12%.

201 Zone LH-3 (~ 1450-150 cal yr BP) is subdivided in two subzones. Subzone 3A (~1450-600 cal yr BP) is  
202 characterized by an increase in herbaceous pollen, led by Poaceae (~35% maximum during this zone),  
203 Asteraceae (~60% maximum during this zone after ~1000 cal yr BP) and *Artemisia* (~10%), with the  
204 resulting decrease in AP. Since this zone to the Present, *Quercus* pollen is the major component of AP  
205 instead of *Pinus*. Cyperaceae also show a decrease, and Ranunculaceae reach ~ 5%. Subzone 3B (~600-  
206 150 cal yr BP) documents an increase in *Olea* (~6%), Poaceae (20%), Caryophyllaceae (7%) and *Artemisia*  
207 (~2-20%). *Pinus* (~2%) and Asteraceae (~20%) decrease in this period. Aquatic and wetland pollen show  
208 a rise (Cyperaceae ~30%, Rannunculaceae ~10%).

209 Zone LH-4 (~ 150 cal yr BP-present) depicts a further increase in *Olea* (~25%), Poaceae (~40%) and  
210 *Artemisia* (~10%).

#### 211 4.4. Sediment composition

212 The XRF-scanning method relies on determining the relative variations on elements composition.  
213 Nevertheless, due to the presence of major variations in organic matter or carbonates it is necessary to  
214 normalize the measured count in order to obtain an environmentally relevant signal (Löwemark et al.,  
215 2011). Aluminium and titanium normalizations are commonly used to discern possible fluctuations in the  
216 lithogenic fraction (enrichment or depletion of specific elements), particularly in the terrigenous  
217 aluminosilicate sediment fraction (Van der Weijden, 2002; Calvert and Pedersen 2007; Martinez-Ruiz et al.  
218 et al., 2015). For this study, the XRF data were normalized to Ti since Al counts obtained were very low. Poor  
219 detection of Al can be related to either low Al content, or high organic and water contents that increase  
220 radiation absorption and affect the intensity of this light element, among other possibilities (e.g. Tjallingii  
221 et al., 2007).

222 Since data spacing is different between the analyses on discrete samples and the XRF scanner, a linear  
223 interpolation was performed with the purpose of equalizing the space of the different time series (150-300  
224 years). Afterwards, the mobile average was worked out along the time series (taking into account the 5  
225 nearest points) in order to easily identify trends by means of smoothing out data irregularities. The obtained  
226 data were compared, and both XRF-scanner and discrete sample data showed a good correlation. As a

227 consequence, the geochemical proxies displayed higher time resolution than the discrete samples (Table 2).  
228 Discrete sample and XRF data results are described together in order to simplify this section (Fig. 4).  
229 The lower part of the core is typified by maximum values of K/Al and K/Ti ratios, coinciding with the  
230 lowest values in Ca/Al, Ca/Ti and Zr/Al ratios. Pb/Al data show a stable pattern during this interval.  
231 Nevertheless, between 10000 and 9000 cal yr BP and ~8200 cal yr BP the trends were reversed, with  
232 relatively low K/Al, low K/Ti and slightly increasing Zr/Al, Ca/Al and Ca/Ti ratios. A positive peak in  
233 Pb/Al ratio at ~8200 cal yr BP is also observed.  
234 Between ~7000 and 4000 cal yr BP a decreasing trend in K/Al and K/Ti ratios occurs along with an  
235 increasing trend in Zr/Al, Ca/Al and Ca/Ti ratios. The Pb/Al ratio remains constant throughout this interval.  
236 From ~4000 to ~2600 cal yr BP an increase in Zr/Al, Ca/Al and Ca/Ti ratios is documented. A maximum  
237 in eolian proxies occurs at ~2600 cal yr BP. A K/Al and K/Ti minima occurs between ~3000 and ~2600 cal  
238 yr BP. The Pb/Al ratio shows a positive peak at ~2800 cal yr BP.  
239 The interval between ~2600 and ~1450 cal yr BP is characterized by low Ca/Al, Ca/Ti and Zr/Al ratios,  
240 with relatively high K/Al and K/Ti ratios. The Pb/Al ratio shows a flat pattern, increasing at ~1500 cal yr  
241 BP.  
242 The period between ~1450 and ~650 cal yr BP depicts higher ratios of Zr/Al, Ca/Al and Ca/Ti and  
243 decreasing ratios of K/Al and K/Ti. A somewhat higher Pb/Al ratio is also registered during this interval.  
244 From ~650 to ~150 low values of Zr/Al and Ca/Ti ratios and minimum values Ca/Al ratio occur. Higher  
245 K/Al and K/Ti values are also observed. The Pb/Al ratio decreases during this interval. From ~150 to the  
246 present, an increase in Zr/Al, Ca/Al, Ca/Ti, K/Ti and a Pb/Al maximum occur. Lower K/Al ratio is recorded  
247 during this period.  
248 Several studies have demonstrated that PCA analysis of geochemical data can elucidate the importance of  
249 different geochemical components driving the environmental responses in marine and lacustrine records  
250 (Bahr et al., 2014; Yuan, 2017). We performed a PCA analysis of the LH geochemical data, which yielded  
251 two significant components (Fig. 5). The first principal component (PC1) describes 58% of the total  
252 variance. The main negative loadings for PC1 are Rb, Ba, Al, K, Ca, Mg and Sr, while large positive  
253 loadings correspond to Zr and Rare Earth Elements (REE). The second principal component (PC2) explains  
254 17% of the total variance. The main negative loading for PC2 are Fe, Ca, Zr, Mg and Lu. Positive loads  
255 correspond to Al, K, Ba, Sr and other elements.  
256 SEM analyses show an alternation between a lithology rich in rock fragments and another rich in organic  
257 remains. Also, diatom frustules, rich in silica, are particularly abundant since ~6300 cal yr BP to Present.  
258 Other minerals such as zircon, rounded quartz and monazite were also identified (Fig. 6).

## 259 **5. Discussion**

260 Pollen and geochemical proxies have been widely used for reconstructing vegetation changes and  
261 environmental and climate variations in southern Iberia (e.g. Carrión, 2002; Sánchez-Goñi and Fletcher,  
262 2008; Anderson et al., 2011; Nieto-Moreno et al., 2011; Jiménez-Moreno et al., 2012; Moreno et al., 2012;  
263 Fletcher and Zielhofer, 2013; Jiménez-Espejo et al., 2014; Ramos-Román et al., 2016). Variations in the  
264 occurrences of arboreal taxa such as *Pinus* and other mesic species (e.g. *Betula*, *Quercus*), indicating  
265 relative humid and warm conditions, and xerophytic species (e.g., Poaceae, Asteraceae, Amaranthaceae,

266 *Artemisia*), representing aridity, have been useful for reconstructing relative humidity changes in southern  
267 Iberian (e.g. Carrión et al., 2001, 2007, 2010; Anderson et al., 2011; Jiménez-Moreno et al., 2012, 2013,  
268 2015; Ramos-Román et al., 2016). *Pinus* reach percentages over 80% in our record. This bisaccate pollen  
269 grain is favoured by wind transport and has a larger dispersal area than other tree species, and sometimes  
270 might be overrepresented (Poska and Pidek, 2010; Pérez-Díaz et al., 2016). Nevertheless, LH is located at  
271 2899 masl only 99 m above treeline and the upper boundary of the oromediterranean belt (1900-2800 masl)  
272 where *Pinus sylvestris* is the main tree specie (El Aallali et al., 1998; Valle, 2003). Therefore, this  
273 apparently anomalous high concentration of *Pinus* may be caused by an upward migration of the  
274 oromediterranean belt and treeline towards higher elevations and around the LH during warmer and more  
275 humid periods, which could have been overstated due to its high pollen-production and dispersal. Therefore,  
276 *Pinus* seems to be mostly recording a regional climatic signal, without allocthonous influence.

277 Over 75% of the total geochemical data variance is explained by the PC1 and PC2 (Fig. 5). We interpret  
278 the results of PC1 as resulting from certain sorting between heavy minerals (positive loading; Zr and REE)  
279 vs. clay minerals and feldspars (negative loadings; K, Al and Ca). The drainage basin is composed mainly  
280 by mica schist, consequently enhanced in K-rich minerals such as mica and feldspar (Díaz de Federico et  
281 al., 1980). This sorting between heavy minerals (enriched in Zr and REE) and clays and feldspars (enriched  
282 in K and Al) (Fig. 5a), was probably linked to physical weathering within the basin and to resulting runoff  
283 until final deposition in the lake.

284 On the other hand, we interpret the results of PC2 as differentiating autochthonous elements (positive  
285 loadings) vs. Saharan allocthonous input (negative loadings). In the first case, due to the abundance of  
286 mica schist within the LH drainage basin (Díaz de Federico et al., 1980), the K/Al and K/Ti ratios are  
287 interpreted as detrital products, and thus a proxy of runoff. In the second case, PC2 negative loading Zr,  
288 Ca, Mg and Fe (Fig. 5b) grouped elements that are coherent with Saharan input composition (dolomite,  
289 iron oxides and heavy minerals) (Ávila, 1997; Morales-Baquero et al., 2006b; Moreno et al., 2006; Pulido-  
290 Villena et al., 2007). In addition, Ca shows a strong positive correlation with Zr since 6300 cal yr BP ( $r$   
291  $=0.57$ ;  $p<0.05$ ) supporting an eolian origin of the Ca in LH sediments. Although we cannot exclude others  
292 nearby Ca sources or changes in the source of African dust (Moreno et al., 2006), the 85% of dust reaching  
293 south Iberia derives from the Sahara (Morales-Baquero and Pérez-Martínez, 2016; Jiménez et al., 2018).  
294 For instance, enrichment in heavy minerals such as zircon and palygorskite has previously been used as an  
295 eolian proxy in the western Mediterranean (e.g., Combourieu Nebout et al., 2002, Rodrigo-Gámiz et al.,  
296 2011, 2015). High concentrations of Ca in other lacustrine systems is usually associated with biogenic  
297 sources when anti-correlated with terrigenous elements (Yuan, 2017). Nevertheless, elevated Ca in the LH  
298 record is linked with detrital elements, as shown by PC1, where Ca is associated with K and Al (Fig. 5a).  
299 Therefore Ca/Al and Ca/Ti ratios are used in the LH record as Saharan eolian input proxies.

300 Elemental ratio variations, such as the ratios K/Al and K/Ti indicating fluvial input and the ratios Zr/Al or  
301 Zr/Th indicating aridity and eolian input, have been previously interpreted in Alboran Sea marine records  
302 as well as in southern Iberia lake records (Martín-Puertas et al., 2010; Nieto-Moreno et al., 2011, 2015;  
303 Rodrigo-Gámiz et al., 2011; Jiménez-Espejo et al., 2014; Martínez-Ruiz et al., 2015; García-Alix et al.,  
304 2017, 2018). Thus, the integration of both palynological data and geochemical ratios used as detrital input  
305 from LH have allowed the reconstruction of the palaeoclimate and palaeoenvironmental history in Sierra



306 Nevada during the Holocene.

## 307 **5.1. Holocene palaeoclimate and palaeoenvironmental history**

### 308 **5.1.1. Early and Mid-Holocene humid conditions (10800–7000 cal yr BP)**

309 The wettest conditions are recorded during the Early Holocene in Sierra Nevada. This is shown in the LH  
310 record by the highest K/Al ratio and MS values, and the low values in Zr/Al, Ca/Al and Ca/Ti ratios,  
311 suggesting that runoff dominated over eolian processes at this time (zone LH-1; Fig. 7) and agrees with  
312 previous studies in the area (Anderson et al., 2011; Jiménez-Moreno and Anderson, 2012; García-Alix et  
313 al., 2012; Jiménez-Espejo et al., 2014). Unfortunately, the pollen record from LH during this interval is  
314 insufficient to definitely confirm this interpretation, due to the high detrital sediment composition and low  
315 organic content, as shown by the low MS values and low pollen preservation. However, high percentages  
316 of AP in two out of three analysed samples suggest humid conditions and high runoff during this period,  
317 and maybe an upward migration of the oromediterranean belt inferred by the high *Pinus* percentages.

318 An Early Holocene humid stage is noticed in other nearby sites, such as the south-faced Laguna de Río Seco  
319 (LdRS; Fig. 1) (Anderson et al., 2011), when the highest lake level of the Holocene occurred. This is also  
320 coeval with the dominance of arboreal species such as *Pinus* as well as aquatic and wetland plants  
321 (Anderson et al., 2011). Low eolian input, noted by geochemical ratios, is also recorded in LdRS during  
322 this interval (Jiménez-Espejo et al., 2014). Further indications of elevated humidity come from the north-  
323 facing Borreguil de la Virgen (BdIV) (see Fig. 1), which is dominated by an AP assemblage and a high  
324 occurrence of aquatic algae *Pediastrum* along with a higher lake level (Jiménez-Moreno et al., 2012).

325 Although the preponderance of evidence accumulated for the Early Holocene suggests overall humid  
326 conditions, at least three relatively arid periods are identified with the geochemical data in the LH record  
327 (Fig. 7). The first arid period occurred between ~9600 and 9000 cal yr BP, the second occurred ~8200 cal  
328 yr BP and the third around 7500 cal yr BP.

329 The first arid event is characterized in LH by a decrease in K/Al and K/Ti ratios and MS, resulting from the  
330 lower runoff input with the concomitant change to a more peaty composition. This event could be correlated  
331 with a dryness event recorded in the Siles Lake record (Carrion, 2002) at ~9300 cal yr BP noticed by an  
332 increase in *Pseudoschizaea*, which was coeval with a minor decrease in arboreal pollen also recorded in  
333 several sites in North Iberia (Iriarte-Chiapusso et al., 2016). At marine site ODP 976 (Fig.1; Combourieu-  
334 Nebout et al., 2009) a decrease in deciduous *Quercus* occurred between 9500 and 9200 cal yr BP indicating  
335 a rapid excursion towards arid conditions (Fig.7). The speleothem record of Corchia Cave also shows dryer  
336 conditions during this interval (Fig. 7; Regattieri et al., 2014) In addition, a decrease in fluvial input in the  
337 Southern Alps and an aridification phase in southeastern France and southeastern Iberia has been similarly  
338 recorded (Jalut et al., 2000).

339 The second dry event recorded at ~8200 cal yr BP is depicted in LH record by a negative peak in K/Ti and  
340 K/Al ratios, and by the onset of a trend toward peatier lithology as evidenced by the MS profile. This event  
341 is not recognized in LH record as clearly as the 9500 cal yr BP and the 7500 cal yr BP dry events. A decrease  
342 in *Pinus* percentage is observed in the nearby LdRS (Anderson et al., 2011), while a forest decrease is  
343 recorded in the Alboran Sea sites MD95-2043 and ODP 976. In several records from north western Iberia,  
344 a decrease in arboreal pollen also occurred at this time (Iriarte-Chiapusso et al., 2016).

345 The 8.2 ka event was the most rapid climate change towards cooler conditions occurred during the  
346 Holocene. It was defined in Greenland ice cores by minimum values in  $\delta^{18}\text{O}$  and affected the North Atlantic  
347 basin and the Mediterranean area (Alley et al., 1997; Rasmussen et al., 2007; Wiersma et al., 2011). Recent  
348 simulations point to a fresh water input in North Atlantic which could slow down the North Atlantic Deep  
349 Water (NADW) formation preventing the heat transport over the north hemisphere (Wiersma et al., 2010,  
350 2011; Young et al., 2013).

351 Another dry event is recorded in LH at  $\sim 7500$  cal yr BP evidenced by the higher peat content in the  
352 sediment, as well as by the lower MS values and a relative minimum in the K/Ti ratio. A relative AP  
353 minimum also occurred in LH at this time. This short-live event is depicted sharper than 8200 cal yr BP  
354 event in several sites in southern Iberia and Alboran Sea: In the Padul record, located at 725 masl at the  
355 lower part of Sierra Nevada a decrease in both evergreen and deciduous *Quercus* is interpreted as a dry and  
356 cold event (Ramos-Román, 2018; Ramos-Román et al., 2018a); forest expansion in Guadiana valley during  
357 the early-mid Holocene is interrupted by a xeric shrublands development between 7850 and 7390 cal yr BP  
358 (Fletcher et al., 2007); in the Alboran Sea a decrease in deciduous *Quercus* is registered at site MD95-2043;  
359 at site 300G a decrease in winter and summer temperatures is also recorded during this interval (Jiménez-  
360 Espejo et al., 2008); in lake Pergusa (south Italy) a trend toward arid conditions began at  $\sim 7500$  cal yr BP  
361 (Magny et al., 2012); in Corchia Cave an arid excursion occurred at  $\sim 7500$  cal yr BP within an overall  
362 humid period between 8300 cal yr BP and 7200 cal yr BP (Fig. 7; Regattieri et al., 2014).

363 Importantly, these arid events recorded in LH at 9600 to 9000 cal yr BP and 8200 cal yr BP are coeval with  
364 the ice-rafted debris events 6 and 5 defined by Bond et al. 1997 in North Atlantic.

### 365 **5.1.2. Mid- and Late Holocene ( $\sim 7000$ cal yr BP-2600 cal yr BP)**

366 The Middle and Late Holocene in the southern Iberian Peninsula is characterized by a trend towards more  
367 arid conditions (Jalut et al., 2009; Anderson et al., 2011; Rodrigo-Gámiz et al., 2011; Jiménez-Moreno and  
368 Anderson, 2012; Jiménez-Espejo et al., 2014). In the LH record an abrupt decrease in the MS values  
369 indicates a lithological change to more peaty sedimentation at  $\sim 7000$  cal yr BP. Similarly, a decrease in the  
370 K/Al and K/Ti ratios, points to a transition to less humidity and runoff (Fig. 7). *Quercus* percentage  
371 increases at this time, partially replacing the *Pinus*, which mainly compose the AP during the record. A  
372 progressive increasing trend in eolian input from Sahara (Zr/Al, Ca/Al and Ca/Ti ratios) is observed around  
373 5500-6500 cal yr BP (Fig. 7), also pointing to an increase in aridity in the area. This change coincides with  
374 regional increases in the Zr/Th ratio (equivalent to Zr/Al ratio) and *Artemisia* pollen, and with decreases in  
375 *Betula* and *Pinus* in the LdRS record (Anderson et al., 2011; Jiménez-Espejo et al., 2014), and in *Pinus* in  
376 the BdIV record (Jiménez-Moreno et al., 2012). Rodrigo-Gámiz et al. (2011) and Jiménez-Espejo et al.  
377 (2014) observed similar geochemical patterns in western Mediterranean marine records and in LdRS, with  
378 a decline in fluvial input, and a decline in surface runoff, respectively. The same pattern is noticed in marine  
379 pollen records MD95-2043 and ODP 976 (Fletcher and Sanchez-Goñi, 2008; Combourieu-Nebout et al.,  
380 2009; Fig. 7). Contemporaneously, aridity is also suggested from speleothem data around the Mediterranean  
381 area: At El Refugio cave, a hiatus in the speleothem growing rate occurred between 7300 and 6100 cal year  
382 BP (Walczak et al., 2015), which is coeval with a drop in  $\delta^{18}\text{O}$  in Soreq (Israel) and Corchia (Italy; CC26;  
383 Fig. 1 and 7) caves at 7000 cal yr BP (Bar-Matthews et al., 2000; Zanchetta et al., 2007; Regattieri et al.,

384 2014). Also at ~7000 cal yr BP a decreasing trend in the deciduous/sclerophyllous pollen ratio occurred in  
385 southeastern France and Iberia (Jalut et al., 2000) and at continental sites around the Mediterranean Sea  
386 (Jalut et al., 2009). In addition, very low lake levels were recorded in the Sahara-Sahel Belt (Liu et al.,  
387 2007) and in the Southern Alps (Magny et al., 2002).

388 Enhanced arid conditions are observed in the LH record between 4000 and 2500 cal yr BP, interpreted  
389 through a decline in AP and a Poaceae maximum. Also a surface runoff minimum and an increase in eolian  
390 input proxies took place between 3500 and 2500 cal yr BP (zone LH-3). In Corchia Cave an arid interval  
391 was recorded at ~3100 cal yr BP (Regattieri et al., 2014), coeval with another one observed globally and  
392 described by Mayewski et al. (2004) between 3500 and 2500 cal yr BP. Nevertheless, this period is not  
393 climatically stable, fluctuations are observed in K/Ti, K/Al, Ca/Ti, Ca/Al and Zr/Al ratios. Furthermore,  
394 peaks in *Quercus* are recorded in LH, LdlM and ODP 976 sites at ~3900 cal yr BP and ~3100 cal yr BP,  
395 when AP in LH decreases (Combourieu-Nebout et al., 2009; Jiménez-Moreno et al., 2013). This fact a  
396 priori contradictory, could be explained by altitudinal displacements of the tree taxa such as *Quercus* in the  
397 oromediterranean belt due to the climatic variability occurred along this interval (Carrión, 2002). During  
398 warmer periods, this species would be displaced towards higher elevation and the influence  
399 of *Quercus* pollen in Sierra Nevada would be larger, this could explain relative higher *Quercus* percentages  
400 in LdlM, LH and also in the ODP 976 record. The same relationship between *Quercus* and *Pinus* is  
401 observed comparing the BdlC and Padul records, located closely but with large altitude difference (BdlC  
402 ~2992 masl; Padul ~725 masl; Ramos-Román, 2018) where is also likely linked to movements in the  
403 oromediterranean belt (Ramos-Román, 2018). These altitudinal displacements of the tree taxa have been  
404 previously related to temperature changes in others southern Iberian records, suggesting an ecological niche  
405 competition between *Pinus* and *Quercus* species at middle altitudes (see Carrión et al., 2002 for a revision).

#### 406 **5.1.3. Iberian Roman Humid Period (IRHP; ~2600-1450 cal yr BP)**

407 Because there is no consensus in the literature about the chronology for the main climatic stages during the  
408 last 2000 years (Muñoz-Sobrino et al., 2014; Helama et al., 2017), here we follow the chronology proposed  
409 by Moreno et al. (2012): Dark Ages (DA, 1450-1050 cal yr BP); Medieval Climate Anomaly (MCA, 1050-  
410 650 cal yr BP); and LIA (650-150 cal yr BP). Another climatic stage precedes the DA – the Iberian Roman  
411 Humid Period (IRHP, 2600-1600 cal yr BP), originally described by Martín-Puertas et al. (2008). However,  
412 in the LH record we have established different IRHP limits (2600-1450), based accordingly to the pollen  
413 zonation (Fig. 3), and coinciding with the DA onset defined by Moreno et al. (2012).

414 The IRHP has been described as the wettest period in the western Mediterranean from proxies determined  
415 both in marine and lacustrine records during the Late Holocene (Reed et al., 2001; Fletcher and Sanchez-  
416 Goñi 2008; Combourieu-Nebout et al., 2009; Martín-Puertas et al., 2009; Nieto-Moreno et al., 2013;  
417 Sánchez-López et al., 2016). A relative maximum in AP occurred in the LH record during this time, also  
418 indicating forest development and relative high humidity during the Late Holocene in the area (zone LH-  
419 4; Fig. 7). This is further supported by high K/Al and K/Ti ratios and MS values, indicating high detrital  
420 input in the drainage basin, a minimum in Poaceae and low Saharan eolian input (low Ca/Al, Ca/Ti and  
421 Zr/Al ratios) (Fig. 7). Fluvial elemental ratios have also shown an increase in river runoff in Alboran Sea  
422 marine records (Nieto-Moreno et al., 2011; Rodrigo-Gámiz et al., 2011). This humid period seems to be  
423 correlated with a solar maximum (Solanki et al., 2004) and persistent negative NAO conditions (Olsen et

424 al., 2012), which could have triggered general humid conditions in the Mediterranean. However, in the LH  
425 record fluctuation in AP between 2300 and 1800 cal yr BP occurred, pointing to arid conditions at that time.  
426 This arid event also seems to show up in BdlC, with a decrease in AP between 2400 and 1900 cal yr BP  
427 (Ramos-Román et al., 2016) and in Zoñar Lake, with water highly chemically concentrated and gypsum  
428 deposition between 2140 and 1800 cal yr BP (Martín-Puertas et al., 2009). In Corchia Cave a rapid  
429 excursion towards arid condition is recoded at ~2000 cal yr BP (Regattieri et al., 2014) (Fig.7). As we  
430 explained in section 5, the apparently anomalous percentages of *Pinus* at this time, could be justified by an  
431 upward migrations of the oromediterranean forest species triggered by higher temperatures and/or the high  
432 pollen-production and dispersal of *Pinus*. Nevertheless, we cannot exclude others factors that could  
433 influence the pollen transport such as the wind energy, mostly controlled by the NAO in the southern Iberia.  
434 A persistent negative NAO phase, as occurred during the IRWP (Sánchez-López et al., 2016), would have  
435 triggered more humid conditions and higher westerlies influence over southern Europe. The higher  
436 occurrence of *Pinus* in the surrounding area due to the favourable climatic conditions, along with the higher  
437 wind energy over Sierra Nevada and the characteristics of bisaccate pollen, could have overstate the  
438 percentages of *Pinus* in our record.

#### 439 **5.1.4. Dark Ages and Medieval Climate Anomaly (DA, MCA; 1450-650 cal yr BP)**

440 Predominantly arid conditions, depicted by high abundance of herbaceous and xerophytic species and an  
441 AP minimum in the LH record, are shown for both DA and MCA (zone LH-5; Fig. 7). This is further  
442 supported in this record by an increase in Saharan eolian input Ca/Al, Ca/Ti and Zr/Al ratios, and by a  
443 decrease in surface runoff, indicated by the K/Al and K/Ti ratios (zone LH-5; Fig. 7). These results from  
444 LH agree with climate estimations of overall aridity modulated by a persistent positive NAO phase during  
445 this period (Trouet et al., 2009; Olsen et al., 2012), also previously noted by Ramos-Román et al. (2016) in  
446 the area (Fig. 7).

447 Generally arid climate conditions during the DA and the MCA have also been previously described in the  
448 LdlM and BdlC records, shown by a decrease in mesophytes and a rise of xerophytic vegetation during that  
449 time (Jiménez-Moreno et al., 2013; Ramos-Román et al., 2016). Several pollen records in south and central  
450 Iberian Peninsula also indicate aridity during the DA and MCA, for example grassland expanded at Cañada  
451 de la Cruz, while in Siles Lake a lower occurrence of woodlands occurred (Carrión, 2002). Also in Címera  
452 Lake low lake level and higher occurrence of xerophytes were recorded (Sánchez-López et al., 2016). Arid  
453 conditions were depicted in Zoñar Lake by an increase in *Pistacia* and heliophytes (i.e., Chenopodiaceae)  
454 and lower lake level (Martín-Puertas et al., 2010). Similar climatic conditions were noticed in the marine  
455 records MD95-2043 and ODP 976 in the Alboran Sea through decreases in forest (Fletcher and Sánchez-  
456 Goñi, 2008; Combourieu-Nebout et al., 2009; Fig. 7). Arid conditions in Basa de la Mora (northern Iberian  
457 Peninsula) occurred during this time, characterized by maximum values of *Artemisia*, and a lower  
458 development of deciduous *Quercus* and aquatic species such as *Potamogeton*, also indicating low lake  
459 water levels (Moreno et al., 2012). Arid conditions were also documented by geochemical data in marine  
460 records from the Alboran Sea (Nieto-Moreno et al., 2013, 2015), in the Gulf of Lion and South of Sicily  
461 (Jalut et al., 2009). Aridity has also been interpreted for central Europe using lake level reconstructions  
462 (Magny, 2004) and in speleothems records in central Italy (Regattieri et al., 2014). Nevertheless, wetter

463 conditions were recorded during the DA in some records from northern Iberian Peninsula (Sánchez-López  
464 et al., 2016). Humid conditions depicted by higher lake level and less salinity occurred in Arreo Lake  
465 (Corella et al., 2013). In Sanabria Lake, the dominance of planktonic diatom *Aulacoseira subborealis* is  
466 interpreted as relative humid conditions at that time (Jambrina-Enríquez et al., 2014). This heterogeneity in  
467 the climate during the DA is due to the existence of an N-S humidity gradient in the Iberian Peninsula  
468 (Sánchez-López et al., 2016). Nonetheless, this gradient seems to be more diffuse during the MCA, which  
469 is characterized as an overall arid period in the entire Iberian Peninsula (Morellón et al., 2012; Sánchez-  
470 López et al., 2016).

#### 471 **5.1.5. Little Ice Age (LIA; 650-150 cal yr BP)**

472 The LIA is interpreted as an overall humid period in the LH record. This is indicated by higher AP values  
473 than during the MCA, low Saharan dust input (low Ca/Al, Ca/Ti and Zr/Al ratios), a decrease in herbs  
474 (Poaceae) and high values in the K/Al and K/Ti ratios indicating enhanced runoff (zone LH-6A; Fig. 7).  
475 An increase in fluvial-derived proxies has been previously documented in other Iberian terrestrial records  
476 such as Basa de la Mora Lake (Moreno et al., 2012), Zoñar Lake (Martín-Puertas et al., 2010) or Cimera  
477 Lake (Sánchez-López et al., 2016) and marine records from the Alboran Sea basin (Nieto-Moreno et al.,  
478 2011, 2015). Lake level reconstructions in Estanya Lake, in the Pre-Pyrenees (NE Spain), have shown high  
479 water levels during this period (Morellón et al., 2009, 2011), supporting our humid climate inferences.  
480 Nevertheless, fluctuations in *Artemisia* during the LIA suggest an unstable period in Sierra Nevada (Fig.  
481 8), in agreement with the high variability in *Pinus*, *Artemisia*, and water availability deduced from recent  
482 high-resolution studies in the neighbour BdlC and BdlV records (Ramos-Román et al., 2016; García-Alix  
483 et al., 2017). The same pattern occurred in several Iberian records (Oliva et al., 2018), revealing that the  
484 LIA was not a climatically stable period and many oscillations at short-time scale occurred.  
485 A persistently negative NAO phase, although with high variability, occurred during this period (Trouet et  
486 al., 2009), which could explain the overall humid conditions observed in southern Europe. As in the Early  
487 Holocene arid events, solar variability has been hypothesized as the main forcing of this climatic event  
488 (Bond et al., 2001; Mayewski et al., 2004; Fletcher et al., 2013; Ramos-Román et al., 2016).

#### 489 **5.2. Industrial Period (IP; 150 cal yr BP-Present)**

490 The IP is characterized by a sharp increase in the Pb/Al ratio in LH record (Fig. 8), suggesting more mining,  
491 fossil fuel burning or other human industrial activities (García-Alix et al., 2013, 2017). This is coeval with  
492 a rise in AP, which is also related to human activities such as *Olea* commercial cultivation at lower  
493 elevations around Sierra Nevada or *Pinus* reforestation in the area (Fig. 7 and 8; Valbuena-Carabaña et al.,  
494 2010; Anderson et al., 2011). The same pattern has also been observed in others records from Sierra Nevada  
495 (Jiménez-Moreno and Anderson, 2012; García-Alix et al., 2013; Ramos-Román et al., 2016), in Zoñar Lake  
496 and the Alboran Sea records (Martín-Puertas et al., 2010). In addition, a progressively increasing trend in  
497 Zr/Al and Ca/Al ratios is observed during the last two centuries, which could be related to increasing local  
498 aridity and/or anthropogenic desertification, but also with a change in the origin and/or composition of the  
499 dust reaching to the lake (Jiménez-Espejo et al., 2014), likely related to the beginning of extensive  
500 agriculture and the concomitant desertification in the Sahel region (Mulitza et al., 2010).

### 501 **5.3 Significance of the eolian record from Laguna Hondera**

502 Saharan dust influence over current alpine lake ecosystems is widely known (Morales-Baquero et al.,  
503 2006a, 2006b; Pulido-Villena et al., 2008b; Mladenov et al., 2011, Jiménez et al., 2018). The most  
504 representative elements of Saharan dust in LH record are Fe, Zr and Ca as shown by the PC2 loading (Fig.  
505 5), where Ca and Fe directly affect the alpine lake biogeochemistry in this region (Pulido-Villena et al.,  
506 2006, 2008b, Jiménez et al., 2018). Zirconium is transported in heavy minerals in eolian dust (Govin et al.,  
507 2012) and has largely been used in the Iberian Peninsula and the western Mediterranean as an indicator of  
508 eolian Saharan input (Moreno et al., 2006; Nieto-Moreno et al., 2011; Rodrigo-Gámiz et al., 2011; Jiménez-  
509 Espejo et al., 2014; Martínez-Ruiz et al., 2015, and references therein). High Zr content has also been  
510 identified in present aerosols at high elevations in Sierra Nevada (García-Alix et al., 2017). Considering  
511 the low weatherable base cation reserves in LH bedrock catchment area, calcium is suggested to be carried  
512 by atmospheric input of Saharan dust into alpine lakes in Sierra Nevada (Pulido-Villena et al., 2006, see  
513 discussion; Morales-Baquero et al., 2013). This is the first time that the Ca signal is properly recorded in a  
514 long record from Sierra Nevada. This could be explained by higher evaporation rates at this site promoting  
515 annual lake desiccation that could prevent Ca water column dissolution and using/recycling by organism,  
516 preserving better the original eolian signal. These elements have an essential role as nutrients becoming  
517 winnowed and recycled rapidly in the oligotrophic alpine lake ecosystem (Morales-Baquero et al., 2006b).  
518 This phenomenon has also been observed in other high-elevation lakes where the phytoplankton is  
519 supported by a small and continually recycled nutrient pool (e.g., Sawatzky et al., 2006).

520 The SEM observations further confirm the presence of Saharan dust in the lake sediments from LH and the  
521 occurrence of Zircon, the main source of eolian Zr, which is relatively abundant (Fig. 6a). Quartz with  
522 rounded morphologies (eolian erosion) are also frequent (Fig. 6b) in the uppermost part of the record as  
523 well as REE rich minerals, such as monazite, which is typical from the Saharan-Sahel Corridor area  
524 (Moreno et al., 2006) (Fig. 6c). In addition, the fact that the highest correlation between Ca and Zr occurred  
525 after ~6300 cal yr BP, ( $r=0.57$   $p<0.005$ ) along with the SEM observation and the low availability of Ca in  
526 these ecosystems, could suggest that the beginning of Saharan dust arrivals to the lake including both  
527 elements took place at this time, giving rise to the present way of nutrient inputs in these alpine lakes  
528 (Morales-Baquero et al., 2006b; Pulido-Villena et al., 2006). The onset of Saharan dust input into southern  
529 Iberia occurred prior to the end of the African Humid Period (AHP; ~5500 cal yr BP; deMenocal et al.,  
530 2000), as previously noticed in the nearby LdRS (Jiménez-Espejo et al., 2014) and in Alboran Sea (Rodrigo-  
531 Gámiz et al., 2011). This could suggest a progressive climatic deterioration in North Africa, which  
532 culminated with the AHP demise and the massive Saharan dust input recorded in all records in Sierra  
533 Nevada at ~3500 cal yr BP (Fig. 7).

### 534 **6. Conclusions**

535 The multiproxy paleoclimate analysis from LH has allowed the reconstruction of the vegetation and climate  
536 evolution in Sierra Nevada and southern Iberia during the Holocene, and the possible factors that have  
537 triggered paleoenvironmental changes. Climate during the Early Holocene was predominantly humid, with  
538 two relatively arid periods between 10000 and 9000 and at ~8200 cal yr BP, resulting in less detrital inputs  
539 and a change to more peaty lithology. The onset of an arid trend took place around 7000 cal yr BP,

540 decreasing the runoff input in the area. A significant increase in eolian-derived elements occurred between  
541 6300 and 5500 cal yr BP, coinciding with the AHP demise. An arid interval is recorded between 4000 and  
542 2500 cal yr BP, with a vegetation assemblage dominated by xerophytes.  
543 Relative humid conditions occurred in the area between 2500 and 1450 cal yr BP, interrupting the Late  
544 Holocene aridification trend. This humid interval was characterized by expansion of forest vegetation, high  
545 runoff input, and a more clayey lithology. However, during the DA and the MCA (1450-650 cal yr BP)  
546 there was enhanced eolian input and an expansion of xerophytes, indicating increased arid conditions. In  
547 contrast, the LIA (650-150 cal yr BP) was characterized by predominant humid conditions as pointed out  
548 high runoff and low eolian input. The IP (150 cal yr BP-Present) is characterized in the LH record by the  
549 highest values of the Pb/Al ratio, probably indicating fossil fuel burning by enhanced mining and metallurgy  
550 industry. The increase in human activities at this time in this area can also be deduced by the expansion of  
551 *Olea* cultivation at lower elevations and *Pinus* reforestation in the area.  
552 Importantly, the LH record shows a unique and exceptional Ca signal derived from eolian input (high Ca-  
553 Zr correlation) during the past ~6300 years in Sierra Nevada. The good preservation of the Ca record might  
554 have been favoured by the high evaporation and the low lake depth, which could have prevented Ca column  
555 water dissolution and its re-use by organisms. Our record indicate that present-day inorganic nutrient input  
556 from Sahara was established 6300 yrs ago and lasted until the present, with variations depending on the  
557 prevailing climate.

## 558 **Acknowledgements**

559 This study was supported by the project P11-RNM 7332 of the “Junta de Andalucía”, the projects  
560 CGL2013-47038-R, CGL2015-66830-R of the “Ministerio de Economía y Competitividad of Spain and  
561 Fondo Europeo de Desarrollo Regional FEDER”, the research groups RNM0190 and RNM179 (Junta de  
562 Andalucía). We also thank to Unidad de Excelencia (UCE-PP2016-05). J.M.M.F acknowledges the PhD  
563 funding provided by Ministerio de Economía y Competitividad (CGL2015-66830-R) A.G.-A. was also  
564 supported by a Marie Curie Intra-European Fellowship of the 7th Framework Programme for Research,  
565 Technological Development and Demonstration of the European Commission (NAOSIPUK. Grant  
566 Number: PIEF-GA-2012-623027) and by a Ramón y Cajal Fellowship RYC-2015-18966 of the Spanish  
567 Government (Ministerio de Economía y Competitividad) and M.R.G. from the Andalucía Talent Hub  
568 Program co-funded by the European Union’s Seventh Framework Program (COFUND – Grant Agreement  
569 n° 291780) and the Junta de Andalucía. We thank Santiago Fernández, Maria Dolores Hernandez and  
570 Antonio Mudarra for their help recovering the core and Inés Morales for the initial core description and MS  
571 data. We thank Jaime Frigola (Universitat de Barcelona) for his help with XRF core scanning.

## 572 **References**

573 Anderson, R. S., Jiménez-Moreno, G., Carrión, J. S., and Pérez-Martínez, C.: Holocene vegetation history  
574 from Laguna de Río Seco, Sierra Nevada, southern Spain, Quaternary Sci. Rev. 30, 1615-1629,  
575 DOI:10.1016/j.quascirev.2011.03.005, 2011.

576 Andrade, A., Valdeolmillos, A., and Ruíz-Zapata, B.: Modern pollen spectra and contemporary vegetation  
577 in the Paramera Mountain range (Ávila, Spain), *Rev. Palaeobot. Palyno.*, 82, 127-139, DOI:10.1016/0034-  
578 6667(94)90024-8, 1994.

579 Ariztegui, D., Asioli, A., Lowe, J. J., Trincardi, F., Vigliotti, L., Tamburini, F., Chondrogianni, C., Accorsi,  
580 C. A., Bandini Mazzanti, M., Mercuri, A. M., Van der Kaars, S., McKenzie, J. A., and Oldfield, F.:  
581 Palaeoclimate and the formation of sapropel S1: inferences from Late Quaternary lacustrine and marine  
582 sequences in the central Mediterranean region, *Palaeogeogr. Palaeocl.*, 158, 215-240, DOI:10.1016/S0031-  
583 0182(00)00051-1, 2000.

584 Aubet, M. E.: *The Phoenicians and the West: Politics, colonies and trade*, Cambridge University Press,  
585 Cambridge, 2001.

586 Ávila, A., Queralt-Mitjans, I., and Alarcón, M.: Mineralogical composition of African dust delivered by  
587 red rains over northeastern Spain, *J. Geophys. Res.-Atmos.*, 102, 21977-21996, DOI:10.1029/97JD00485,  
588 1997.

589 Ballantyne, A. P., Brahney, J., Fernandez, D., Lawrence, C. L., Saros, J., and Neff, J. C.: Biogeochemical  
590 response of alpine lakes to a recent increase in dust deposition in the Southwestern US, *Biogeosciences*, 8,  
591 2689, DOI:10.5194/bg-8-2689-2011, 2011.

592 Bar-Matthews, M., Ayalon, A., and Kaufman, A.: Timing and hydrological conditions of sapropel events  
593 in the Eastern Mediterranean, as evident from speleothems, Soreq cave, Israel, *Chem. Geol.*, 169, 145-156,  
594 DOI:10.1016/S0009-2541(99)00232-6, 2000.

595 Bahr, A., Jiménez-Espejo, F. J., Kolasinac, N., Grunert, P., Hernández-Molina, F. J., Röhl, U., Voelker, A.  
596 H. L., Escutia, C., Stow, D. A. V., Hodell, D., and Alvarez-Zarikian, C. A.: Deciphering bottom current  
597 velocity and paleoclimate signals from contourite deposits in the Gulf of Cádiz during the last 140 kyr: An  
598 inorganic geochemical approach, *Geochem. Geophys. Geosy.*, 15, 3145-3160,  
599 DOI:10.1002/2014GC005356, 2014.

600 Blaauw, M.: Methods and code for 'classical' age-modelling of radiocarbon sequences, *Quat. Geochronol.*,  
601 5, 512-518, DOI:10.1016/j.quageo.2010.01.002, 2010.

602 Bea, F.: Residence of REE, Y, Th and U in granites and crustal protoliths: implications for the chemistry  
603 of crustal melts, *J. Petrol.*, 37, 521-532, DOI:10.1093/petrology/37.3.521, 1996.

604 Beug, H. J.: *Leitfaden der Pollenbestimmung für Mitteleuropa und angrenzende Gebiete*, Fischer, Stuttgart,  
605 2004.

606 Bond, G., Showers, W., Cheseby, M., Lotti, R., Almasi, P., deMenocal, P., Priore, P., Cullen, H., Hajdas,  
607 I., and Bonani, G.: A pervasive millennial-scale cycle in North Atlantic Holocene and glacial climates,  
608 *Science*, 278, 1257-1266, DOI:10.1126/science.278.5341.1257, 1997.

609 Bond, G., Kromer, B., Beer, J., Muscheler, R., Evans, M., Showers, W., Hoffmann, S., Lotti-Bond, R.,  
610 Hajdas, I., and Bonani, G.: Persistent solar influence on North Atlantic climate during the Holocene,  
611 *Science*, 294, 2130-2136, DOI:10.1126/science.1065680, 2001.



612 Cacho, I., Grimalt, J. O., and Canals, M.: Response of the Western Mediterranean Sea to rapid climatic  
613 variability during the last 50,000 years: a molecular biomarker approach, *J. Marine Syst.*, 33-34, 253-272,  
614 DOI:10.1016/S0924-7963(02)00061-1, 2002.

615 Calvert, S. E., and Pedersen, T. F.: Elemental proxies for palaeoclimatic and palaeoceanographic variability  
616 in marine sediments: interpretation and application, *Proxies in Late Cenozoic Paleoceanography*, Elsevier,  
617 Amsterdam, 2007.

618 Carrión, J. S.: Patterns and processes of Late Quaternary environmental change in a montane region of  
619 southwestern Europe, *Quaternary Sci. Rev.*, 21, 2047-2066, DOI:10.1016/S0277-3791(02)00010-0, 2002.

620 Carrión, J. S., Munuera, M., Dupré, M., and Andrade, A.: Abrupt vegetation changes in the Segura  
621 mountains of southern Spain throughout the Holocene, *J. Ecol.*, 89, 783-797, DOI:10.1046/j.0022-  
622 0477.2001.00601.x, 2001.

623 Carrión, J. S., Sánchez-Gómez, P., Mota, J. F., Yll, E. I., and Chaín, C.: Fire and grazing are contingent on  
624 the Holocene vegetation dynamics of Sierra de Gádor, southern Spain, *Holocene* 13, 839-849,  
625 DOI:10.1191/0959683603hl662rp, 2003.

626 Carrión, J. S., Fuentes, N., González-Sampériz, P., Sánchez Quirante, L., Finlayson, J. C., Fernández, S.,  
627 and Andrade, A.: Holocene environmental change in a montane region of southern Europe with a long  
628 history of human settlement, *Quaternary Sci. Rev.*, 26, 1455-1475, DOI:10.1016/j.quascirev.2007.03.013,  
629 2007.

630 Carrión, J. S., Fernández, S., González-Sampériz, P., Gil-Romera, G., Badal, E., Carrión-Marco, Y., López-  
631 Merino, L., López-Sáez, J. A., Fierro, E., and Burjachs, F.: Expected trends and surprises in the Lateglacial  
632 and Holocene vegetation history of the Iberian Peninsula and Balearic Islands, *Rev. Palaeobot. Palyno.*,  
633 162, 458-476, DOI:10.1016/j.jaridenv.2008.11.014, 2010.

634 Castillo Martín, A.: *Lagunas de Sierra Nevada*, Universidad de Granada, Granada, 2009.

635 Combourieu Nebout, N., Turon, J. L., Zahn, R., Capotondi, L., Londeix, L., and Pahnke, K.: Enhanced  
636 aridity and atmospheric high-pressure stability over the western Mediterranean during the North Atlantic  
637 cold events of the past 50 ky, *Geology*, 30, 863-866, DOI:10.1130/0091-  
638 7613(2002)030<0863:EAAAHP>2.0.CO;2, 2002..

639 Combourieu Nebout, N., Peyron, O., Dormoy, I., Desprat, S., Beaudouin, C., Kotthoff, U., and Marret, F.:  
640 Rapid climatic variability in the west Mediterranean during the last 25,000 years from high resolution pollen  
641 data, *Clim. Past*, 5, 503-521, DOI:10.5194/cpd-5-671-2009, 2009.

642 Comero, S., Locoro, G., Free, G., Vaccaro, S., De Capitani, L., and Gawlik, B. M.: Characterisation of  
643 Alpine lake sediments using multivariate statistical techniques, *Chemometr. Intell. Lab.*, 107(1), 24-30,  
644 DOI:10.1016/j.chemolab.2011.01.002, 2011.

645 Corella, J. P., Stefanova, V., El Anjoumi, A., Rico, E., Giralt, S., Moreno, A., Plata-Monter, A., and Valero-  
646 Garcés, B. L.: A 2500-year multi-proxy reconstruction of climate change and human activities in northern  
647 Spain: the Lake Arreo record, *Palaeogeogr. Palaeoclimatol. Palaeoecol.*, 386, 555-568,  
648 DOI:10.1016/j.palaeo.2013.06.022, 2013.

649 Davis, J. C., and Sampson, R. J.: *Statistics and data analysis in geology*, Wiley, New York, 1986.

650 de Lange, G. J., Thomson, J., Reitz, A., Slomp, C. P., Principato, M. S., Erba, E., and Corselli, C.:  
651 Synchronous basin-wide formation and redox-controlled preservation of a Mediterranean sapropel, *Nat.*  
652 *Geosci.*, 1, 606-610, DOI:10.1038/ngeo283, 2008.

653 deMenocal, P., Ortiz, J., Guilderson, T., Adkins, J., Sarnthein, M., Baker, L., and Yarusinsky, M.: Abrupt  
654 onset and termination of the African Humid Period: rapid climate responses to gradual insolation forcing,  
655 *Quaternary Sci. Rev.*, 19, 347-361, DOI:10.1016/S0277-3791(99)00081-5, 2000.

656 Díaz de Federico, A.: *Estudio geológico del Complejo de Sierra Nevada en la transversal del Puerto de la*  
657 *Ragua (Cordillera Bética)*, Ph.D. thesis, Universidad de Granada, Granada, 1980.

658 El Aallali, A., López Nieto, J. M., Pérez Raya, F., and Molero Mesa, J.: Estudio de la vegetación forestal  
659 en la vertiente sur de Sierra Nevada (Alpujarra Alta granadina), *Itinera Geobot.*, 11, 387-402, 1998.

660 Faegri, K., and Iversen, J.: *Textbook of Pollen Analysis*, Wiley, New York, 1989.

661 Fletcher, W. J., Boski, T., and Moura, D.: Palynological evidence for environmental and climatic change  
662 in the lower Guadiana valley, Portugal, during the last 13 000 years, *Holocene*, 17, 481-494,  
663 DOI:10.1177/0959683607077027, 2007.

664 Fletcher, W. J., and Sánchez Goñi, M. F.: Orbital- and sub-orbital-scale climate impacts on vegetation of  
665 the western Mediterranean basin over the last 48,000 yr, *Quaternary Res.*, 70, 451-464,  
666 DOI:10.1016/j.yqres.2008.07.002, 2008.

667 Fletcher, W. J., Sánchez Goñi, M. F., Peyron, O., and Dormoy, I.: Abrupt climate changes of the last  
668 deglaciation detected in a Western Mediterranean forest record, *Clim. Past*, 6, 245-264, DOI:10.5194/cp-  
669 6-245-2010, 2010.

670 Fletcher, W. J., and Zielhofer, C.: Fragility of Western Mediterranean landscapes during Holocene rapid  
671 climate changes, *Catena*, 103, 16-29, DOI:10.1016/j.catena.2011.05.001, 2013.

672 García-Alix, A., Jiménez-Moreno, G., Anderson, R. S., Jiménez-Espejo, F. J., and Delgado-Huertas, A.:  
673 Holocene paleoenvironmental evolution of a high-elevation wetland in Sierra Nevada, southern Spain,  
674 deduced from an isotopic record, *J. Paleolimnol.*, 48, 471-484, DOI:10.1007/s10933-012-9625-2 , 2012.

675 García-Alix, A., Jiménez-Espejo, F. J., Lozano, J. A., Jiménez-Moreno, G., Martínez-Ruiz, F., García  
676 Sanjuán, L., Aranda Jiménez, G., García Alfonso, E., Ruiz-Puertas, G., and Anderson, R. S.: Anthropogenic  
677 impact and lead pollution throughout the Holocene in Southern Iberia, *Sci. Total Environ.*, 449, 451-460,  
678 DOI:10.1016/j.scitotenv.2013.01.081, 2013.

679 García-Alix, A., Jimenez Espejo, F. J., Toney, J. L., Jiménez-Moreno, G., Ramos-Román, M. J., Anderson,  
680 R. S., Ruano, P., Queralt, I., Delgado Huertas, A., and Kuroda, J.: Alpine bogs of southern Spain show  
681 human-induced environmental change superimposed on long-term natural variations, *Sci. Rep.-UK*, 7,  
682 7439, DOI:10.1038/s41598-017-07854-w, 2017.

683 García-Alix, A., Jiménez-Espejo, F.J., Jiménez-Moreno, G., Toney, J.L., Ramos-Román, M.J., Camuera,  
684 J., Anderson, R.S., Delgado-Huertas, A., Martínez-Ruiz, F., and Queralt, I.: Holocene geochemical

685 footprint from Semi-arid alpine wetlands in southern Spain, *Sci. Data*, 5, 180024,  
686 DOI:10.1038/sdata.2018.24, 2018.

687 Govin, A., Holzwarth, U., Heslop, D., Ford Keeling, L., Zabel, M., Mulitza, S., Collins, J. A., and Chiessi,  
688 C. M.: Distribution of major elements in Atlantic surface sediments (36°N-49°S): imprint of terrigenous  
689 input and continental weathering, *Geochem. Geophys. Geosy.*, 13, Q01013, DOI:10.1029/2011GC003785,  
690 2012.

691 Grimm, E. C.: CONISS: a Fortran 77 program for stratigraphically constrained cluster analysis by the  
692 method of incremental sum of squares, *Comput. Geosci.*, 13, 13-35, DOI:10.1016/0098-3004(87)90022-7,  
693 1987.

694 Grimm, E.: TILIA: a pollen program for analysis and display, Illinois State Museum, Springfield, 1993.

695 Hammer, Ø., Harper, D. A. T., and Ryan, P. D.: Paleontological Statistics Software Package for Education  
696 and Data Analysis, *Palaeontol. electron.*, 4, 1-9, 2001.

697 Harper, D. A. T.: Numerical Palaeobiology, John Wiley & Sons, Chichester, 1999.

698 Helama, S., Jones, P. D., and Briffa, K. R.: Dark Ages Cold Period: A literature review and directions for  
699 future research, *Holocene* 27, 1600-1606, DOI: 10.1177/0959683617693898, 2017.

700 Jalut, G., Esteban Amat, A., Bonnet, L., Gauquelin, T., and Fontugne, M.: Holocene climatic changes in  
701 the Western Mediterranean, from south-east France to south-east Spain, *Palaeogeogr. Palaeoclimatol.*, 160, 255-  
702 290, DOI:10.1016/S0031-0182(00)00075-4, 2000.

703 Jalut, G., Dedoubat, J. J., Fontugne, M., and Otto, T.: Holocene circum-Mediterranean vegetation changes:  
704 climate forcing and human impact, *Quatern. Int.*, 200, 4-18, DOI:10.1016/j.quaint.2008.03.012, 2009.

705 Jambrina-Enrriquez, M., Rico, M., Moreno, A., Leira, M., Bernárdez, P., Prego, R., Recio, C., and Valero-  
706 Garcés, B. L.: Timing of deglaciation and postglacial environmental dynamics in NW Iberia: the Sanabria  
707 Lake record, *Quaternary Sci. Rev.*, 94, 136-158, DOI:10.1016/j.quascirev.2014.04.018, 2014.

708 Jiménez, L., Rühland, K. M., Jeziorski, A., Smol, J. P., and Pérez-Martínez, C.: Climate change and Saharan  
709 dust drive recent cladoceran and primary production changes in remote alpine lakes of Sierra Nevada,  
710 Spain, *Glob. Change Biol.*, 24, e139-e158, DOI:10.1111/gcb.13878, 2018.

711 Jiménez-Espejo, F. J., Martínez-Ruiz, F., Rogerson, M., González-Donoso, J. M., Romero, O., Linares, D.,  
712 Sakamoto, T., Gallego-Torres, D., Rueda Ruiz, J. L., Ortega-Huertas, M., and Perez Claros, J. A.: Detrital  
713 input, productivity fluctuations, and water mass circulation in the westernmost Mediterranean Sea since the  
714 Last Glacial Maximum, *Geochem. Geophys. Geosy.*, 9, Q11U02, DOI:10.1029/2008GC002096, 2008.

715 Jiménez-Espejo, F. J., García-Alix, A., Jiménez-Moreno, G., Rodrigo-Gámiz, M., Anderson, R. S.,  
716 Rodríguez-Tovar, F. J., Martínez-Ruiz, F., Giral, S., Delgado-Huertas, A., and Pardo-Igúzquiza, E.:  
717 Saharan aeolian input and effective humidity variations over western Europe during the Holocene from a  
718 high altitude record, *Chem. Geol.*, 374, 1-12, DOI:10.1016/j.chemgeo.2014.03.001, 2014.

- 719 Jiménez-Moreno, G., and Anderson, R. S.: Holocene vegetation and climate change recorded in alpine bog  
720 sediments from the Borreguiles de la Virgen, Sierra Nevada, southern Spain, *Quaternary Res.*, 77, 44-53,  
721 DOI:10.1016/j.yqres.2011.09.006, 2012.
- 722 Jiménez-Moreno, G., García-Alix, A., Hernández-Corbalán, M. D., Anderson, R. S., and Delgado-Huertas,  
723 A.: Vegetation, fire, climate and human disturbance history in the southwestern Mediterranean area during  
724 the late Holocene, *Quaternary Res.*, 79, 110-122, DOI:10.1016/j.yqres.2012.11.008, 2013.
- 725 Jiménez-Moreno, G., Rodríguez-Ramírez, A., Pérez-Asensio, J. N., Carrión, J. S., López-Sáez, J. A.,  
726 Villarías-Robles, J. J. R., Celestino-Pérez, S., Cerrillo-Cuenca, E., Ángel León, A., and Contreras, C.:  
727 Impact of late-Holocene aridification trend, climate variability and geodynamic control on the environment  
728 from a coastal area in SW Spain, *Holocene*, 25, 607-617, DOI:10.1177/0959683614565955, 2015.
- 729 Lionello, P., Malanotte-Rizzoli, P., Boscolo, R., Alpert, P., Artale, V., Li, L., Luterbacher, J., May, W.,  
730 Trigo, R., Tsimplis, M., Ulbrich, U., and Xoplaki, E.: The Mediterranean climate: an overview of the main  
731 characteristics and issues, *Developments in Earth and Environmental Sciences*, 4, Elsevier, Amsterdam,  
732 Netherlands, 1-26, 2006.
- 733 Liu, Z., Wang, Y., Gallimore, R., Gasse, F., Johnson, T., deMenocal, P., Adkins, J., Notaro, M., Prentice,  
734 I. C., Kutzbach, J., Jacob, R., Behling, P., Wang, L., and Ong, E.: Simulating the transient evolution and  
735 abrupt change of Northern Africa atmosphere–ocean–terrestrial ecosystem in the Holocene. *Quaternary*  
736 *Sci. Rev.*, 26, 1818-1837, DOI:10.1016/j.quascirev.2007.03.002, 2007.
- 737 Löwemark, L., Chen, H.-F., Yang, T.-N., Kylander, M., Yu, E.-F., Hsu, Y.-W., Lee, T.-Q., Song, S.-R.,  
738 and Jarvis, S.: Normalizing XRF-scanner data: a cautionary note on the interpretation of high-resolution  
739 records from organic-rich lakes, *J. Asian Earth Sci.*, 40, 1250-1256, DOI:10.1016/j.jseaes.2010.06.002,  
740 2011.
- 741 Magny, M., Miramont, C., and Sivan, O.: Assessment of the impact of climate and anthropogenic factors  
742 on Holocene Mediterranean vegetation in Europe on the basis of palaeohydrological records, *Palaeogeogr.*  
743 *Palaeocl.*, 186, 47-59, DOI:10.1016/S0031-0182(02)00442-X, 2002.
- 744 Magny, M., and Bégeot, C.: Hydrological changes in the European midlatitudes associated with freshwater  
745 outbursts from Lake Agassiz during the Younger Dryas event and the early Holocene, *Quaternary Res.*, 61,  
746 181-192, doi:10.1016/j.yqres.2003.12.003, 2004.
- 747 Magny, M., de Beaulieu, J.-L., Drescher-Schneider, R., Vannière, B., Walter-Simonnet, A.-V., Miras, Y.,  
748 Millet, L., Bossuet, G., Peyron, O., Brugiapaglia, E., and Leroux, A.: Holocene climate changes in the  
749 central Mediterranean as recorded by lake-level fluctuations at Lake Accessa (Tuscany, Italy), *Quaternary*  
750 *Sci. Rev.*, 26, 1736-1758, DOI:10.1016/j.quascirev.2007.04.014, 2007.
- 751 Magny, M., Peyron, O., Sadori, L., Ortu, E., Zanchetta, G., Vannière, B., and Tinner, W.: Contrasting  
752 patterns of precipitation seasonality during the Holocene in the south- and north-central Mediterranean, *J.*  
753 *Quat. Sci.*, 27, 290-296, DOI:10.1002/jqs.1543, 2012.

754 Martín-Puertas, C., Valero-Garcés, B. L., Mata, M. P., González-Sampéris, P., Bao, R., Moreno, A., and  
755 Stefanova, V.: Arid and humid phases in southern Spain during the last 4000 years: the Zonar Lake record,  
756 Cordoba, Holocene, 18, 907-921, DOI:10.1177/0959683608093533, 2008.

757 Martín-Puertas, C., Valero-Garcés, B. L., Brauer, A., Mata, M. P., Delgado-Huertas, A., and Dulski, P.:  
758 The Iberian–Roman Humid Period (2600–1600 cal yr BP) in the Zoñar Lake varve record (Andalucía,  
759 southern Spain), Quaternary Res., 71, 108-120, DOI:10.1016/j.yqres.2008.10.004, 2009.

760 Martín-Puertas, C., Jiménez-Espejo, F., Martínez-Ruiz, F., Nieto-Moreno, V., Rodrigo, M., Mata, M. P.,  
761 and Valero-Garcés, B. L.: Late Holocene climate variability in the southwestern Mediterranean region: an  
762 integrated marine and terrestrial geochemical approach, Clim. Past, 6, 807-816, DOI:10.5194/cp-6-807-  
763 2010, 2010.

764 Martínez-Ruiz, F., Kastner, M., Gallego-Torres, D., Rodrigo-Gámiz, M., Nieto-Moreno, V., and Ortega-  
765 Huertas, M.: Paleoclimate and paleoceanography over the past 20,000 yr in the Mediterranean Sea Basins  
766 as indicated by sediment elemental proxies, Quaternary Sci. Rev., 107, 25-46,  
767 DOI:10.1016/j.quascirev.2014.09.018, 2015.

768 Mayewski, P. A., Rohling, E. E., Curt Stager, J., Karlén, W., Maasch, K. A., David Meeker, L., Meyerson,  
769 E. A., Gasse, F., van Kreveld, S., Holmgren, K., Lee-Thorp, J., Rosqvist, G., Rack, F., Staubwasser, M.,  
770 Schneider, R. R., and Steig, E. J.: Holocene climate variability, Quaternary Res. 62, 243-255, DOI:  
771 10.1016/j.yqres.2004.07.001, 2004.

772 Mladenov, N., Pulido-Villena, E., Morales-Baquero, R., Ortega-Retuerta, E., Sommaruga, R., and Reche,  
773 I.: Spatiotemporal drivers of dissolved organic matter in high alpine lakes: Role of Saharan dust inputs and  
774 bacterial activity, J. Geophys. Res.-Bioge., 113, DOI:10.1029/2008JG000699, 2008.

775 Mladenov, N., Sommaruga, R., Morales-Baquero, R., Laurion, I., Camarero, L., Diéguez, M. C., Camacho,  
776 A., Delgado, A., Torres, O., Chen, Z., Felip, M., and Reche, I.: Dust inputs and bacteria influence dissolved  
777 organic matter in clear alpine lakes, Nat. Commun. 2, 405, DOI:10.1038/ncomms1411, 2011.

778 Morales-Baquero, R., Carrillo, P., Reche, I., and Sánchez-Castillo, P.: Nitrogen-phosphorus relationship in  
779 high mountain lakes: effects of the size of catchment basins, Can. J. Fish. Aquat. Sci., 56, 1809-1817,  
780 DOI:10.1139/cjfas-56-10-1809, 1999.

781 Morales-Baquero, R., Pulido-Villena, E., and Reche, I.: Atmospheric inputs of phosphorus and nitrogen to  
782 the southwest Mediterranean region: Biogeochemical responses of high mountain lakes, Limnol.  
783 Oceanogr., 51, 830-837, DOI:10.4319/lo.2006.51.2.0830, 2006a.

784 Morales-Baquero R., Pulido-Villena, E., Romera, O., Ortega-Retuerta, E., Conde-Porcuna, J. M., Pérez-  
785 Martínez, C., and Reche, I.: Significance of atmospheric deposition to freshwater ecosystems in the southern  
786 Iberian Peninsula, Limnetica, 25, 171-180, 2006b.

787 Morales-Baquero, R., Pulido-Villena, E., and Reche, I.: Chemical signature of Saharan dust on dry and wet  
788 atmospheric deposition in the south-western Mediterranean region, Tellus B, 65,  
789 DOI:10.3402/tellusb.v65i0.18720, 2013.

790 Morales-Baquero, R., and Pérez-Martínez C.: Saharan versus local influence on atmospheric aerosol  
791 deposition in the southern Iberian Peninsula: Significance for N and P inputs, *Global Biogeochem. Cycles*,  
792 30, 501-513, DOI:10.1002/2015GB005254, 2016.

793 Moreno, A., Pérez, A., Frigola, J., Nieto-Moreno, V., Rodrigo-Gámiz, M., Martrat, B., González-Sampérez,  
794 P., Morellón, M., Martín-Puertas, C., Corella, J. P., Belmonte, A., Sancho, C., Cacho, I., Herrera, G.,  
795 Canals, M., Grimalt, J. O., Jiménez-Espejo, F. J., Martínez-Ruiz, F., Vegas-Villarrúbia, T., and Valero-  
796 Garcés, B. L.: The Medieval Climate Anomaly in the Iberian Peninsula reconstructed from marine and lake  
797 records, *Quaternary Sci. Rev.*, 42, 16-32, DOI:10.1016/j.quascirev.2012.04.007, 2012.

798 Moreno, T., Querol, X., Castillo, S., Alastuey, A., Cuevas, E., Herrmann, L., Mounkaila, M., Elvira, J.,  
799 Gibbons, W.: Geochemical variations in aeolian mineral particles from the Sahara–Sahel Dust Corridor.  
800 *Chemosphere*, 65, 261-270, DOI:10.1016/j.chemosphere.2006.02.052, 2006.

801 Morellón, M., Valero-Garcés, B., Vegas-Vilarrúbia, T., González-Sampérez, P., Romero, O., Delgado-  
802 Huertas, A., Mata, P., Moreno, A., Rico, M., and Corella, J. P.: Lateglacial and Holocene palaeohydrology  
803 in the western Mediterranean region: the Lake Estanya record (NE Spain), *Quaternary Sci. Rev.*, 28, 2582-  
804 2599, DOI:10.1016/j.quascirev.2009.05.014, 2009.

805 Morellón, M., Valero-Garcés, B., González-Sampérez, P., Vegas-Vilarrúbia, T., Rubio, E., Rieradevall, M.,  
806 Delgado-Huertas, A., Mata, P., Romero, O., Engstrom, D. R., López-Vicente, M., Navas, A., and Soto, J.:  
807 Climate changes and human activities recorded in the sediments of Lake Estanya (NE Spain) during the  
808 Medieval Warm Period and Little Ice Age, *J. Paleolimnol.*, 46, 423-452, DOI:10.1007/s10933-009-9346-  
809 3, 2011.

810 Morellón, M., Pérez-Sanz, A., Corella, J. P., Büntgen, U., Catalán, J., González-Samprizé, P., González-  
811 Trueba, J. J., López-Sáez, J. A., Moreno, A., Pla, S., Saz-Sánchez, M. Á., Scussolini, P., Serrano, E.,  
812 Steinhilber, F., Stefanova, V., Vegas-Vilarrúbia, T., and Saz-Sánchez, M. A.: A multi-proxy perspective  
813 on millennium-long climate variability in the Southern Pyrenees, *Clim. Past*, DOI:10.5194/cpd-7-3049-  
814 2011, 2012.

815 Mulitza, S., Heslop, D., Pittauerova, D., Fischer, H. W., Meyer, I., Stuut, J.-B., Zabel, M., Mollenhauer,  
816 G., Collins, J.A., Kuhnert, H., and Schulz, M.: Increase in African dust flux at the onset of commercial  
817 agriculture in the Sahel region, *Nature*, 466, 226-228, DOI:10.1038/nature09213, 2010.

818 Sobrino, C. M., García-Moreiras, I., Castro, Y., Carreño, N. M., de Blas, E., Rodríguez, C. F., Judd, A., and  
819 García-Gil, S., Climate and anthropogenic factors influencing an estuarine ecosystem from NW Iberia: new  
820 high resolution multiproxy analyses from San Simón Bay (Ría de Vigo), *Quaternary Sci. Rev.*, 93, 11-33,  
821 DOI:10.1016/j.quascirev.2014.03.021, 2014.

822 Nieto-Moreno, V., Martínez-Ruiz, F., Giralt, S., Jiménez-Espejo, F. J., Gallego-Torres, D., Rodrigo-Gámiz,  
823 M., García-Orellana, J., Ortega-Huertas, M., and de Lange, G. J.: Tracking climate variability in the western  
824 Mediterranean during the Late Holocene: a multiproxy approach, *Clim. Past*, 7, 1395-1414,  
825 DOI:10.5194/cp-7-1395-2011, 2011.

- 826 Nieto-Moreno, V., Martínez-Ruiz, F., Willmott, V., García-Orellana, J., Masqué, P., and Damsté, J. S.:  
827 Climate conditions in the westernmost Mediterranean over the last two millennia: An integrated biomarker  
828 approach, *Org. Geochem.*, 55, 1-10. DOI:10.1177/0959683613484613, 2013
- 829 Nieto-Moreno, V., Martínez-Ruiz, F., Gallego-Torres, D., Giralt, S., García-Orellana, J., Masqué, P.,  
830 Sinninghe Damsté, J. S., and Ortega-Huertas, M.: Palaeoclimate and palaeoceanographic conditions in the  
831 westernmost Mediterranean over the last millennium: an integrated organic and inorganic approach, *J. Geol.*  
832 *Soc. London*, 172, 264-271, DOI: 10.1144/jgs2013-105, 2015.
- 833 Oliva, M., Ruiz-Fernández, J., Barriendos, M., Benito, G., Cuadrat, J. M., Domínguez-Castro, F., García-  
834 Ruiz, J. M., Giralt, S., Gómez-Ortiz, A., Hernández, A., López-Costas, O., López-Moreno, J. I., López-  
835 Sáez, J. A., Matínez-Cortízar, A., Moreno, A., Prohom, M., Saz, M. A. Serrano, E., Tejedor, E., Trigo, R.,  
836 Valero-Garcés, B. and López-Costas, O.: The Little Ice Age in Iberian mountains, *Earth-Sci. Rev.*, 177,  
837 175-208, DOI:10.1016/j.earscirev.2017.11.010, 2018.
- 838 Olsen, J., Anderson, N. J., and Knudsen, M. F.: Variability of the North Atlantic Oscillation over the past  
839 5,200 years, *Nat. Geosci.*, 5, 808-812, DOI:10.1038/ngeo1589, 2012.
- 840 Palma, P., Oliva, M., García-Hernández, C., Ortiz, A. G., Ruiz-Fernández, J., Salvador-Franch, F., and  
841 Catarineu, M.: Spatial characterization of glacial and periglacial landforms in the highlands of Sierra Nevada  
842 (Spain), *Sci. Total Environ.*, 584, 1256-1267, DOI:10.1016/j.scitotenv.2017.01.196, 2017.
- 843 Poska, A., and Pidek, I. A.: Pollen dispersal and deposition characteristics of *Abies alba*, *Fagus sylvatica*  
844 and *Pinus sylvestris*, Roztocze region (SE Poland). *Veg. Hist. Archaeobot.*, 19, 91-101,  
845 DOI:10.1007/s00334-009-0230-x, 2010.
- 846 Pulido-Villena, E., Reche, I., and Morales-Baquero, R.: Significance of atmospheric inputs of calcium over  
847 the southwestern Mediterranean region: High mountain lakes as tools for detection, *Global Biogeochem.*  
848 *Cy.*, 20, GB2012, DOI:10.1029/2005GB002662, 2006.
- 849 Pulido-Villena, E., Wagener, T., and Guieu, C.: Bacterial response to dust pulses in the western  
850 Mediterranean: Implications for carbon cycling in the oligotrophic ocean, *Global Biogeochem. Cy.*, 22,  
851 DOI:10.1029/2007GB003091, 2008a.
- 852 Pulido-Villena, E., Reche, I., and Morales-Baquero, R.: Evidence of an atmospheric forcing on  
853 bacterioplankton and phytoplankton dynamics in a high mountain lake, *Aquat. sci.*, 70, 1-9,  
854 DOI:10.1007/s00027-007-0944-8, 2008b.
- 855 Ramos-Román, M. J., Jiménez-Moreno, G., Anderson, R. S., García-Alix, A., Toney, J. L., Jiménez-Espejo,  
856 F. J., and Carrión, J. S.: Centennial-scale vegetation and North Atlantic Oscillation changes during the Late  
857 Holocene in the southern Iberia, *Quaternary Sci. Rev.*, 143, 84-95, DOI:10.1016/j.quascirev.2016.05.007,  
858 2016.
- 859 Ramos-Román, M. J.: Holocene paleoenvironmental change, climate and human impact in Sierra Nevada,  
860 Southern Iberian Peninsula, Ph. D. Thesis, Universidad de Granada, Granada, 2018.
- 861 Ramos-Román, M. J., Jiménez-Moreno, G., Camuera, J., García-Alix, A., Anderson, R. S., Jiménez-Espejo,  
862 F. J., Sasche, D., Toney, J. L., Carrión, J. S., Webster, C and Yanes, Y.: Millennial-scale cyclical

863 environment and climate variability during the Holocene in the western Mediterranean region deduced from  
864 a new multi-proxy analysis from the Padul record (Sierra Nevada, Spain), *Glob. Planet. Change*, 168, 35-  
865 53, DOI:10.1016/j.gloplacha.2018.06.003, 2018a.

866 Ramos-Román, M. J., Jiménez-Moreno, G., Camuera, J., García-Alix, A., Anderson, R. S., Jiménez-Espejo,  
867 F. J., and Carrión, J. S.: Holocene climate aridification trend and human impact interrupted by millennial-  
868 and centennial-scale climate fluctuations from a new sedimentary record from Padul (Sierra Nevada,  
869 southern Iberian Peninsula), *Clim. Past*, 14, 117-137, DOI:10.5194/cp-14-117-2018, 2018b.

870 Rasmussen, S. O., Vinther, B. M., Clausen, H. B., and Andersen, K. K.: Early Holocene climate oscillations  
871 recorded in three Greenland ice cores, *Quaternary Sci. Rev.*, 26, 1907-1914,  
872 DOI:10.1016/j.quascirev.2007.06.015, 2007.

873 Reche, I., Ortega-Retuerta, E., Romera, O., Villena, E. P., Baquero, R. M., and Casamayor, E. O.: Effect  
874 of Saharan dust inputs on bacterial activity and community composition in Mediterranean lakes and  
875 reservoirs, *Limnol. Oceanogr.*, 54, 869-879, DOI:10.4319/lo.2009.54.3.0869, 2009.

876 Reed, J. M., Stevenson, A. C., and Juggins, S.: A multi-proxy record of Holocene climatic change in  
877 southwestern Spain: the Laguna de Medina, Cádiz, *Holocene*, 11, 707-719, DOI:10.1191/09596830195735,  
878 2001.

879 Reimer, P. J., Bard, E., Bayliss, A., Beck, J. W., Blackwell, P. G., Bronk Ramsey, C., Buck, C. E., Cheng,  
880 H., Edwards, R. L., Friedrich, M., Grootes, P. M., Guilderson, T. P., Haflidason, H., Hajdas, I., Hatté, C.,  
881 Heaton, T. J., Hoffmann, D. L., Hogg, A. G., Hughen, K. A., Kaiser, K. F., Kromer, B., Manning, S. W.,  
882 Niu, M., Reimer, R. W., Richards, D. A., Scott, M., Southon, J. R., Staff, R. A., Turney, C. S. M., and van  
883 der Plicht, J.: IntCal13 and Marine13 radiocarbon age calibration curves 0-50,000 years cal BP,  
884 *Radiocarbon*, 55, 1869-1887, DOI:10.2458/azu\_js\_rc.55.16947, 2013.

885 Regattieri, E., Zanchetta, G., Drysdale, R. N., Isola, I., Hellstrom, J. C., Dallai, L.: Lateglacial to holocene  
886 trace element record (Ba, Mg, Sr) from Corchia cave (Apuan Alps, central Italy): paleoenvironmental  
887 implications, *J. Quat. Sci.*, 29, 381-392, DOI:10.1002/jqs.2712, 2014.

888 Révillon, S., Jouet, G., Bayon, G., Rabineau, M., Dennielou, B., Hémond, C., and Berné, S.: The  
889 provenance of sediments in the Gulf of Lions, western Mediterranean Sea, *Geochem. Geophys. Geosy.*, 12,  
890 Q08006, DOI:10.1029/2011GC003523, 2011.

891 Rodrigo-Gámiz, M., Martínez-Ruiz, F., Jiménez-Espejo, F. J., Gallego-Torres, D., Nieto-Moreno, V.,  
892 Romero, O., Ariztegui, D.: Impact of climate variability in the western Mediterranean during the last 20,000  
893 years: oceanic and atmospheric responses, *Quaternary Sci. Rev.*, 30, 2018-2034,  
894 DOI:10.1016/j.quascirev.2011.05.011, 2011.

895 Sawatzky, C. L., Wurtsbaugh, W. A., Luecke, C.: The spatial and temporal dynamics of deep chlorophyll  
896 layers in high-mountain lakes: effects of nutrients, grazing, and herbivore recycling as growth determinants,  
897 *J. Plankton Res.*, 28, 65–86, DOI:10.1093/plankt/fbi101, 2006.

898 Schulte, L.: Climatic and human influence on river systems and glacier fluctuations in southeast Spain since  
899 the Last Glacial Maximum, *Quatern. Int.*, 93-94, 85-100, DOI:10.1016/S1040-6182(02)00008-3, 2002.



900 Sánchez-López, G., Hernández, A., Pla-Rabes, S., Trigo, R. M., Toro, M., Granados, I., Sáez, A., Masqué,  
901 P., Pueyo, J. J., Rubio-Inglés, M. J., and Giralte, S.: Climate reconstruction for the last two millennia in  
902 central Iberia: The role of East Atlantic (EA), North Atlantic Oscillation (NAO) and their interplay over  
903 the Iberian Peninsula, *Quaternary Sci. Rev.*, 149, 135-150, DOI:10.1016/j.quascirev.2016.07.021, 2016.

904 Settle D. M., and Patterson C. C.: Lead in Albacore: guide to lead pollution in Americans, *Science*, 207,  
905 1167-76, DOI:10.1126/science.6986654 ,1980.

906 Solanki, S. K., Usoskin, I. G., Kromer, B., Schüssler, M., and Beer, J.: Unusual activity of the Sun during  
907 recent decades compared to the previous 11,000 years, *Nature*, 431, 1084-1087, DOI:10.1038/nature02995,  
908 2004.

909 Tjallingii, R., Röhl, U., Kölling, M., and Bickert, T.: Influence of the water content on X-ray fluorescence  
910 core-scanning measurements in soft marine sediments, *Geoch. Geophys. Geosy.*, 8,  
911 DOI:10.1029/2006GC001393, 2007.

912 Trigo, R. M., and Palutikof, J. P.: Precipitation scenarios over Iberia: a comparison between direct GCM  
913 output and different downscaling techniques, *J. Climate* , 14, 4442-4446, DOI:10.1175/1520-  
914 0442(2001)014<4422:PSOIAAC>2.0.CO;2, 2001.

915 Trigo, R. M., Pozo-Vázquez, D., Osborn, T. J., Castro-Díez, Y., Gámiz-Fortis, S., and Esteban-Parra, M.  
916 J.: North Atlantic Oscillation influence on precipitation, river flow and water resources in the Iberian  
917 Peninsula, *Int. J. Climatol.*, 24, 925-944, DOI:10.1002/joc.1048, 2004.

918 Trouet, V., Esper, J., Graham, N. E., Baker, A., Scourse, J. D., and Frank, D. C.: Persistent positive North  
919 Atlantic Oscillation mode dominated the Medieval Climate Anomaly, *Science*, 324, 78-80,  
920 DOI:10.1126/science.1166349, 2009.

921 Valbuena-Carabaña, M., López de Heredia, U., Fuentes-Utrilla, P., González-Doncel, I., and Gil, L.:  
922 Historical and recent changes in the Spanish forests: a socioeconomic process, *Rev. Palaeobot. Palyno.*,  
923 162, 492-506, DOI:10.1016/j.revpalbo.2009.11.003, 2010.

924 Valle, F.: Mapa de series de vegetación de Andalucía 1: 400 000, Editorial Rueda, Madrid, 2003.

925 Van der Weijden, C. H.: Pitfalls of normalization of marine geochemical data using a common divisor,  
926 *Mar. Geol.*, 184, 167-187, DOI:10.1016/S0025-3227(01)00297-3, 2002.

927 Walczak, I. W., Baldini, J. U., Baldini, L. M., McDermott, F., Marsden, S., Standish, C. D., Richards, D.  
928 A., Andreo, B., and Slater, J.: Reconstructing high-resolution climate using CT scanning of unsectioned  
929 stalagmites: A case study identifying the mid-Holocene onset of the Mediterranean climate in southern  
930 Iberia, *Quaternary Sci. Rev.*, 127, 117-128, DOI:10.1016/j.quascirev.2015.06.013, 2015.

931 Wanner, H., Brönnimann, S., Casty, C., Gyalistras, D., Luterbacher, J., Schmutz, C., Stephenson, D. B.,  
932 and Xoplaki, E.: North Atlantic Oscillation—concepts and studies, *Surv. Geophys.*, 22, 321-381,  
933 DOI:10.1023/A:1014217317898, 2001.

934 Wiersma, A. P., and Jongma, J. I.: A role for icebergs in the 8.2 ka climate event, *Climate dynamics*, 35,  
935 535-549, DOI:10.1007/s00382-009-0645-1, 2010.

936 Wiersma, A. P., Roche, D. M., and Renssen, H.: Fingerprinting the 8.2 ka event climate response in a  
937 coupled climate model, *J. Quat. Sci.*, 26, 118-127, DOI:10.1002/jqs.1439, 2011.

938 Yuan, F.: A multi-element sediment record of hydrological and environmental changes from Lake Erie  
939 since 1800, *J. Paleolimnol.*, 58, 23-42, DOI:10.1007/s10933-017-9953-3, 2017.

940 Zanchetta, G., Drysdale, R. N., Hellstrom, J. C., Fallick, A. E., Isola, I., Gagan, M. K., Pareschi, M. T.:  
941 Enhanced rainfall in the Western Mediterranean during deposition of sapropel S1: stalagmite evidence from  
942 Corchia cave (Central Italy), *Quaternary Sci. Rev.*, 26, 279-286, DOI:10.1016/j.quascirev.2006.12.003,  
943 2007.

944

945

946

947

948

949

950

951

952

953

954

955

956

957

958

959

960

961

962

963

964

965

966

967 **List of tables**

<i>Lab Number</i>	<i>Depth (cm)</i>	<i>Dating Method</i>	<i>Age (14C yr BP±1σ)</i>	<i>Calibrated age (cal yr BP)2σ ranges</i>
	0	Present	2012 CE	-63
<i>Poz-72421</i>	7	14C	40±40	29-139
<i>D-AMS 008539</i>	22	14C	1112±32	935-1078
<i>D-AMS 008540</i>	39	14C	2675±30	2750-2809
<i>BETA-411994</i>	44	14C	3350±30	3550-3643
<i>BETA-411995</i>	55.5	14C	5480±30	6261-6318
<i>Poz-72423</i>	57.5	14C	5510±50	6266-6405
<i>Poz-72424</i>	62	14C	6450±50	7272-7433
<i>Poz-72425</i>	74	14C	8620±70	9479-9778

968 **Table 1.** Age data for LH 12-03. All ages were calibrated using IntCal13 curve (Reimer et al., 2013) with  
 969 Clam program (Blaauw, 2010; version 2.2).

970

971

972

973

974

975

976

977

978

979

980

981

982

983

984

985

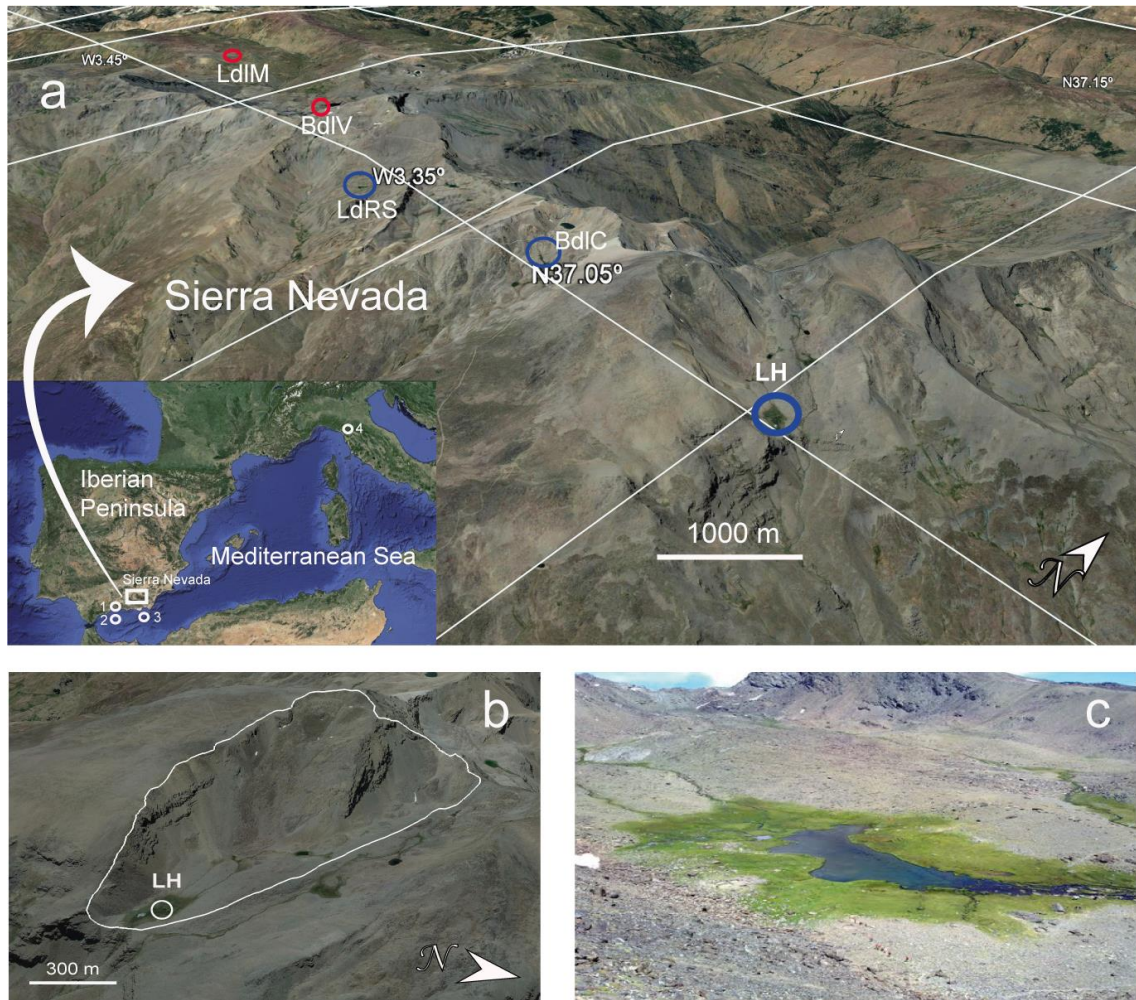
986

987

	Simulation							
Correlation	A		B		C		D	
Ca/Ca (XRF)	0.63	p<0.01	0.50	p<0.01	0.57	p<0.01	0.54	p<0.01
K/K (XRF)	0.53	p<0.01	0.64	p<0.01	0.56	p<0.01	0.65	p<0.01

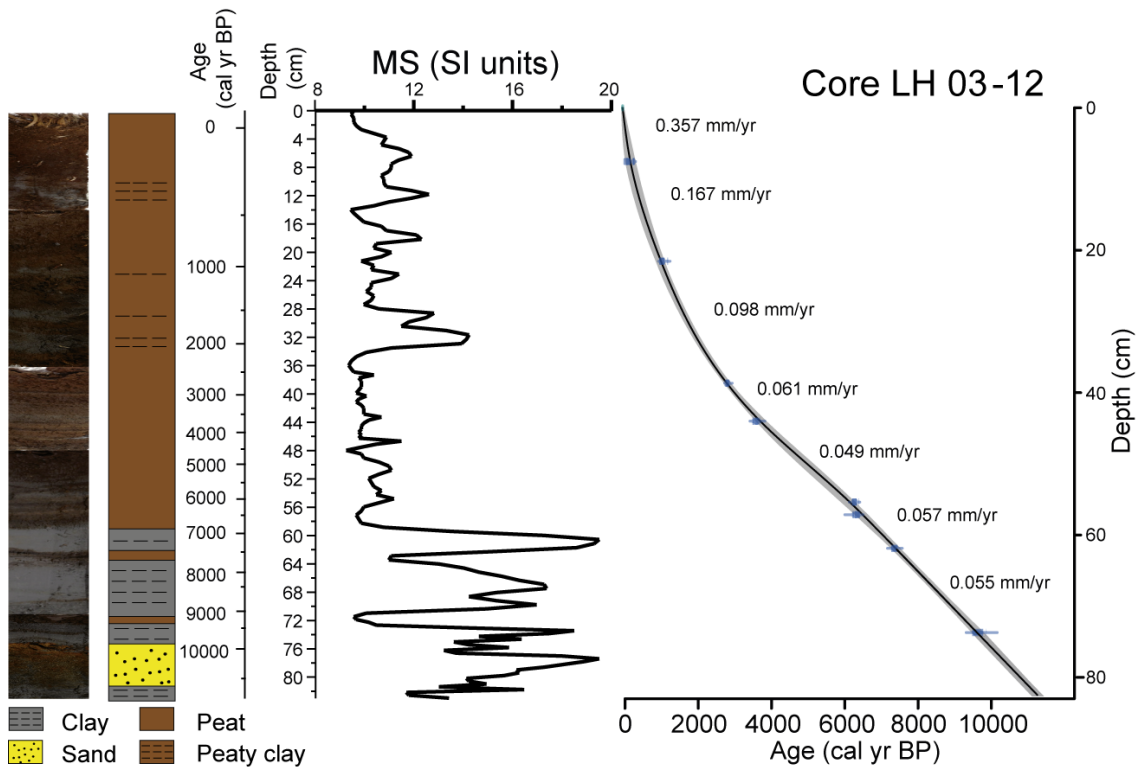
988 **Table 2.** Simulation of proxy correlation. A) regular interpolation of 300 years sampling spacing. B) regular  
989 interpolation of 300 years sampling spacing and 5 data points moving average. C) regular interpolation of  
990 150 years sampling spacing. D) regular interpolation of 150 years sampling spacing and 5 data point moving  
991 average.

992  
993  
994  
995  
996  
997  
998  
999  
1000  
1001  
1002  
1003  
1004  
1005  
1006  
1007  
1008  
1009  
1010  
1011  
1012  
1013  
1014  
1015  
1016  
1017  
1018  
1019



1021

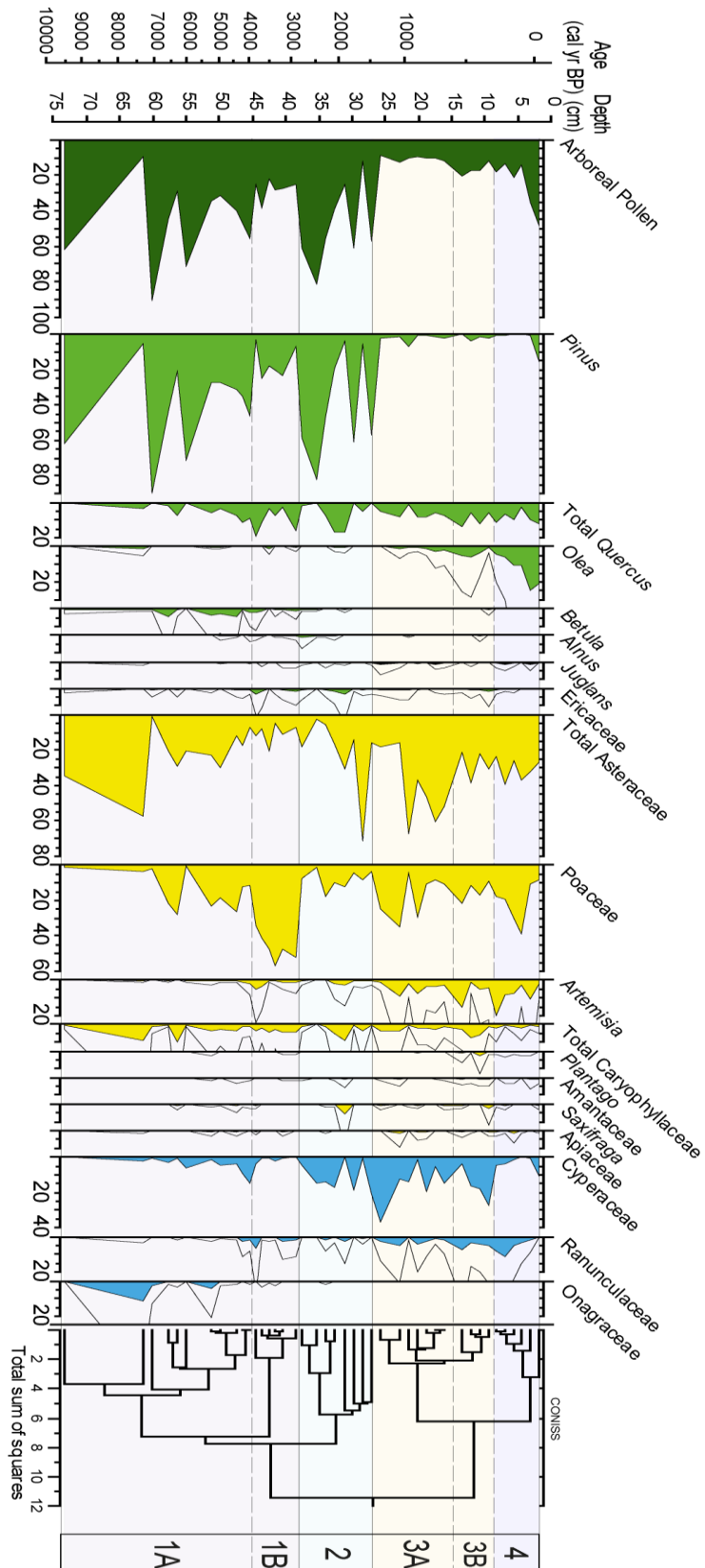
1022 **Figure 1.** (a) Location of the Laguna Hondera (LH) in Sierra Nevada, southern Iberian Peninsula, along  
 1023 with other nearby records mentioned in the text. (1) El Refugio Cave stalagmite record (Walczak et al.,  
 1024 2015); (2) ODP 976 pollen record (Combourieu-Nebout et al., 2009); (3) MD95-2043 pollen record  
 1025 (Fletcher and Sánchez-Goñi, 2008); (4) CC26, Corchia Cave stalagmite record (Zanchetta et al., 2007;  
 1026 Regattieri et al., 2014). Sierra Nevada north-facing sites are encircled in red, south-facing sites are encircled  
 1027 in blue (LH: Laguna Hondera, the current study, is shown in bold). LdLM: Laguna de la Mula (Jiménez-  
 1028 Moreno et al., 2013); BdLV: Borreguil de la Virgen (García-Alix et al., 2012; Jiménez-Moreno and  
 1029 Anderson, 2012); LdRS: Laguna de Río Seco (Anderson et al., 2011; García-Alix et al., 2013; Jiménez-  
 1030 Espejo et al., 2014); BdLC: Borreguil de la Caldera (Ramos-Román et al., 2016; García-Alix et al., 2017)  
 1031 (b) Regional satellite photo of LH. The white line indicates the catchment area. (c) Photo of Laguna  
 1032 Hondera in September 2012, when the core was taken. Photo taken by Gonzalo Jiménez-Moreno. For the  
 1033 coloured figure, we refer the reader to the web version of this article.



1034

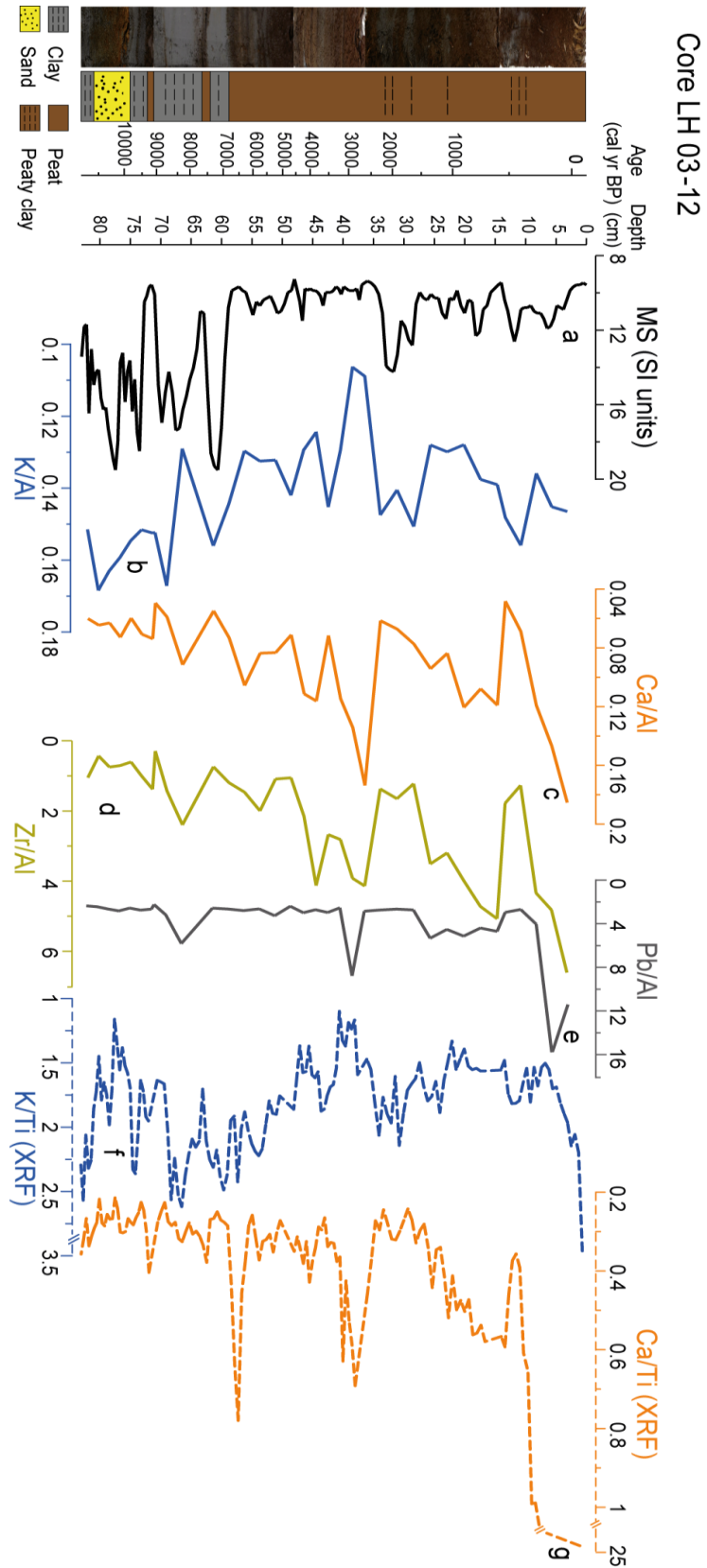
1035 **Figure 2.** Photo of core LH 12-03, along with the lithology, magnetic susceptibility (MS, in SI units) profile  
 1036 and age-depth model. Sediment accumulation rates (SAR in mm yr<sup>-1</sup>) are shown between individual  
 1037 radiocarbon ages, the grey shadow represent the plus/minus range (see details in text for method of  
 1038 construction).

1039



1040

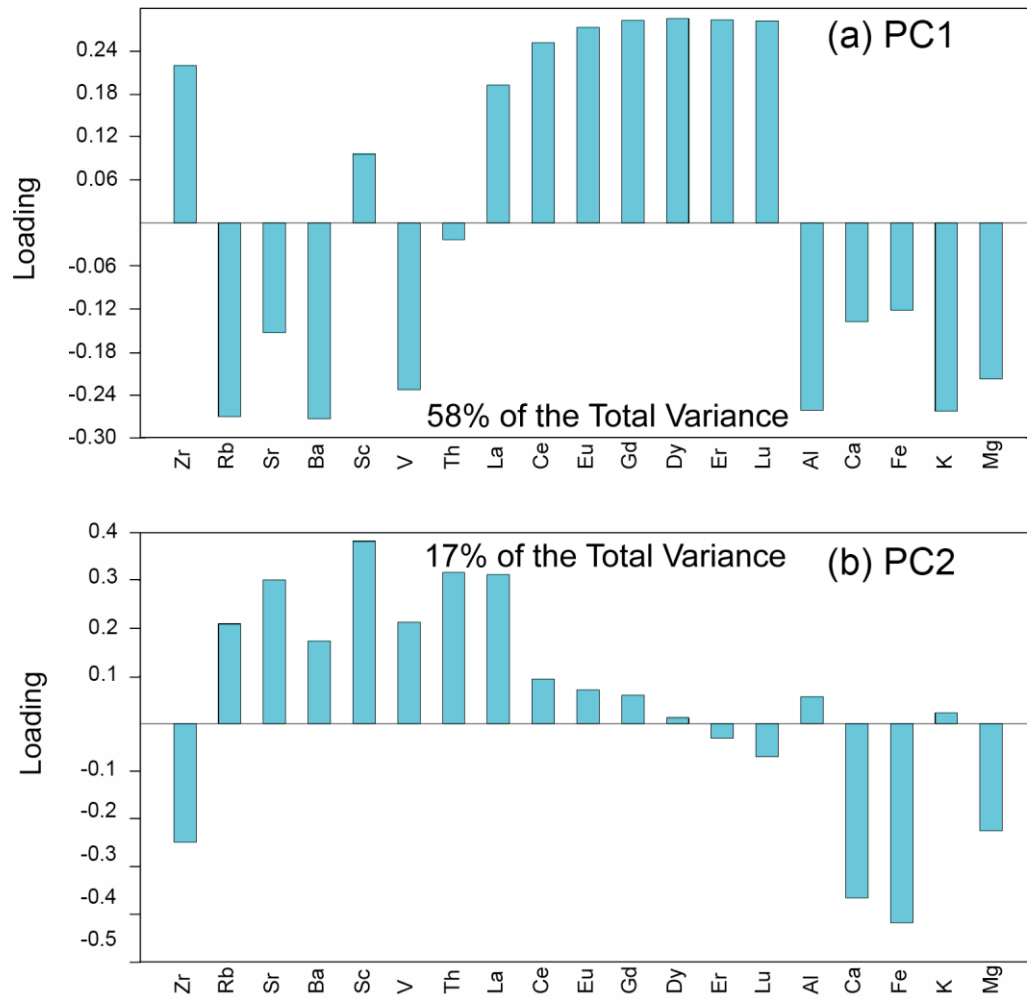
1041 **Figure 3.** Pollen percentage diagram of the LH 12-03 record showing major selected taxa. Major tree  
 1042 species are shown in green; shrubs and herbs are shown in yellow; and wetland and aquatic types are in  
 1043 blue. Pollen was graphed with the Tilia program (Grimm, 1993), and zoned using the CONISS cluster  
 1044 analysis program (Grimm, 1987).



1045

1046 **Figure 4.** Detailed geochemical diagram of the LH 12-03 record showing the selected proxies: (a) MS; (b)  
 1047 K/Al; (c) Ca/Al; (d) Zr/Al; (e) Pb/Al; (f) K/Ti (XRF); (g) Ca/Ti (XRF) (MS in SI units, Zr/Al and Pb/Al  
 1048 scale x 10<sup>-4</sup> and XRF in counts).

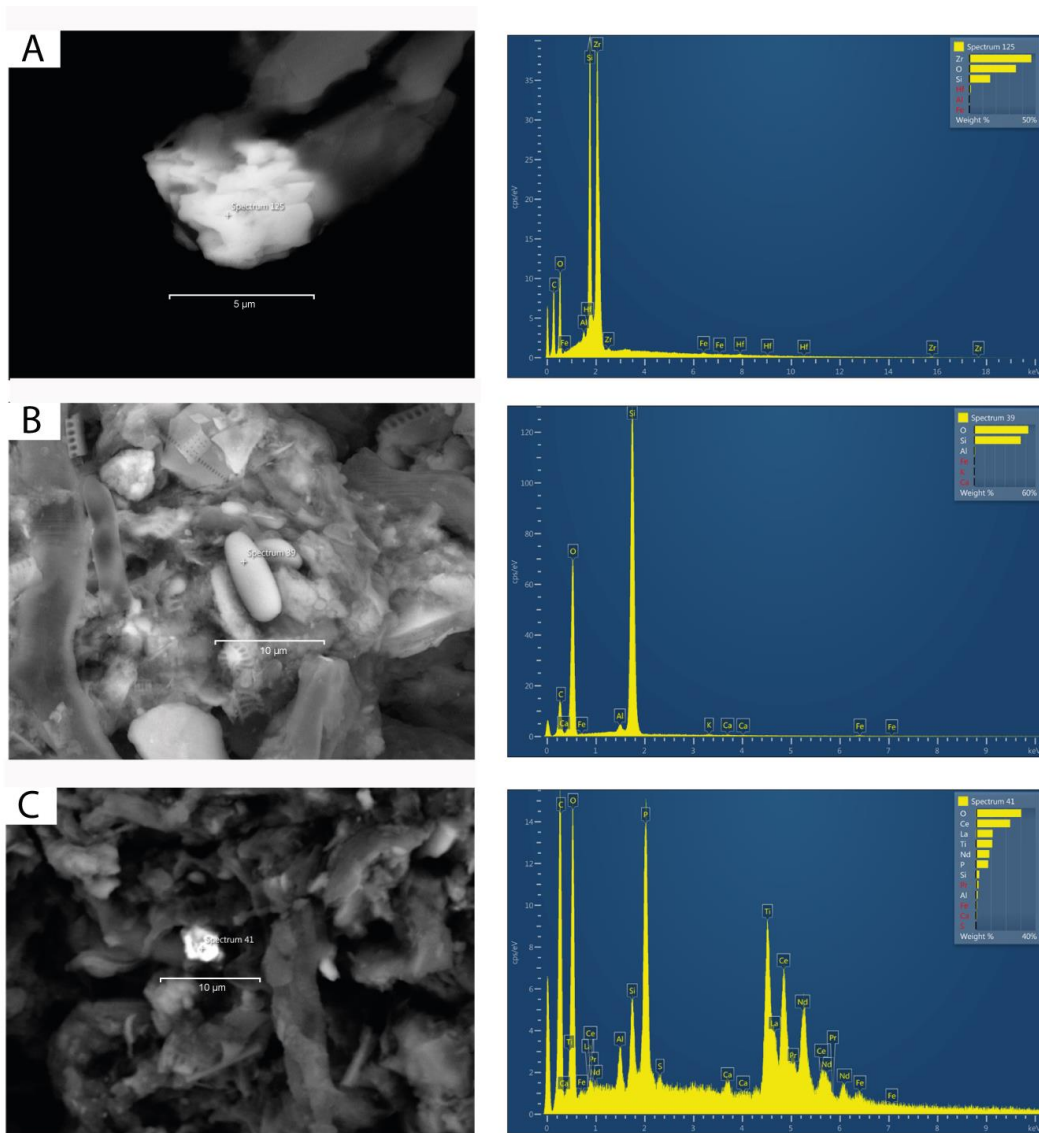




1049

1050 **Figure 5.** Principal Component Analysis (PCA) loadings from selected geochemical elements. (a) PC1,

1051 which describes 58% of total variance; (b) PC2, which describes 17% of total variance.



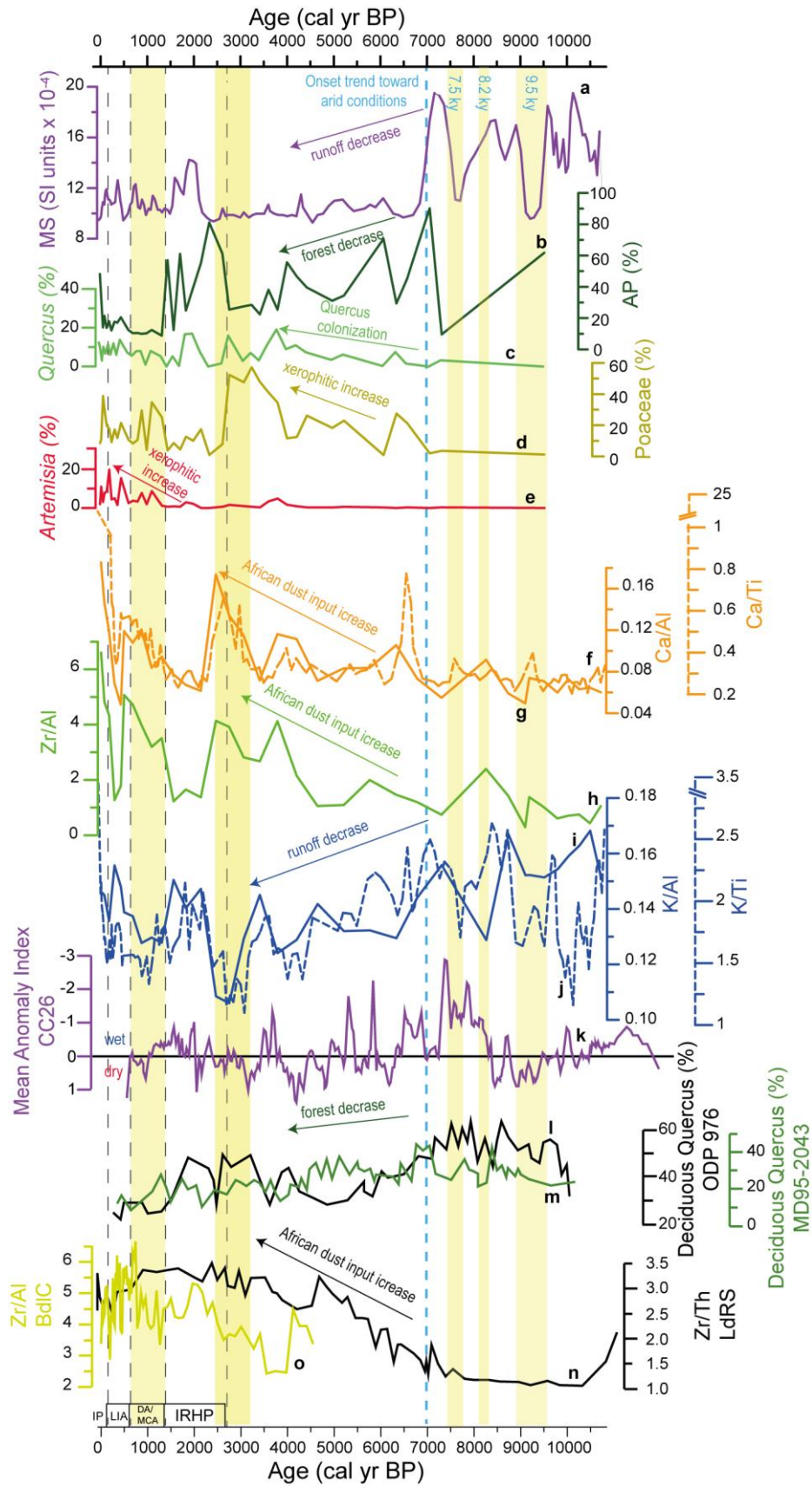
1052

1053

1054

1055

**Figure 6.** Electron Backscatter Diffraction microphotographs of the Laguna Hondera record with clearer colours representing heavier minerals. (a) Zircon, with high Zr content (Dr. 01, 4-5 cm); (b) rounded quartz related with eolian transport (Dr. 01, 2-3 cm); (c) monazite, with high REE content (Dr. 01, 2-3 cm).



1056

1057 **Figure 7.** Comparison between the MS data (in SI units  $\times 10^{-4}$ ), the most important pollen taxa and  
 1058 geochemical proxies from Laguna Hondera (LH) record, with nearby paleoclimate records. (a) LH  
 1059 Magnetic Susceptibility (MS) record; (b) Arboreal Pollen (AP) percentage from LH; (c) *Quercus*

1060 percentage from LH; (d) Poaceae percentage from LH; (e) *Artemisia* percentage from LH; (f) Ca/Ti (XRF)  
1061 ratio from LH in dashed line; (g) Ca/Al ratio from LH; (h) Zr/Al ratio from LH; (i) K/Al ratio from LH; (j)  
1062 K/Ti (XRF) ratio from LH in dashed line; (k) Mean Anomaly Index from CC26 record (Corchia cave;  
1063 Regattieri et al., 2014); (l) Deciduous *Quercus* ODP 976 (Alboran Sea; Combourieu-Nebout et al., 2009);  
1064 (m) Deciduous *Quercus* MD95-2043 (Alboran Sea; Fletcher and Sanchez-Goñi, 2008); (n) Zr/Th ratio from  
1065 Laguna de Río Seco (LdRS) (Jiménez-Espejo et al., 2014; García-Alix et al., 2018); (o) Zr/Al ratio from  
1066 Borreguil de la Caldera (BdlC) (García-Alix et al., 2017; 2018). Yellow bands indicate more arid intervals.  
1067 Dark dashed lines are used for separating the different Current Era periods: IRHP: Iberian Roman Humid  
1068 Period; DA: Dark Ages; MCA: Medieval Climate Anomaly; LIA: Little Ice Age; IP: Industrial Period. Blue  
1069 dashed line indicates the onset of the trend toward arid conditions.

1070

1071

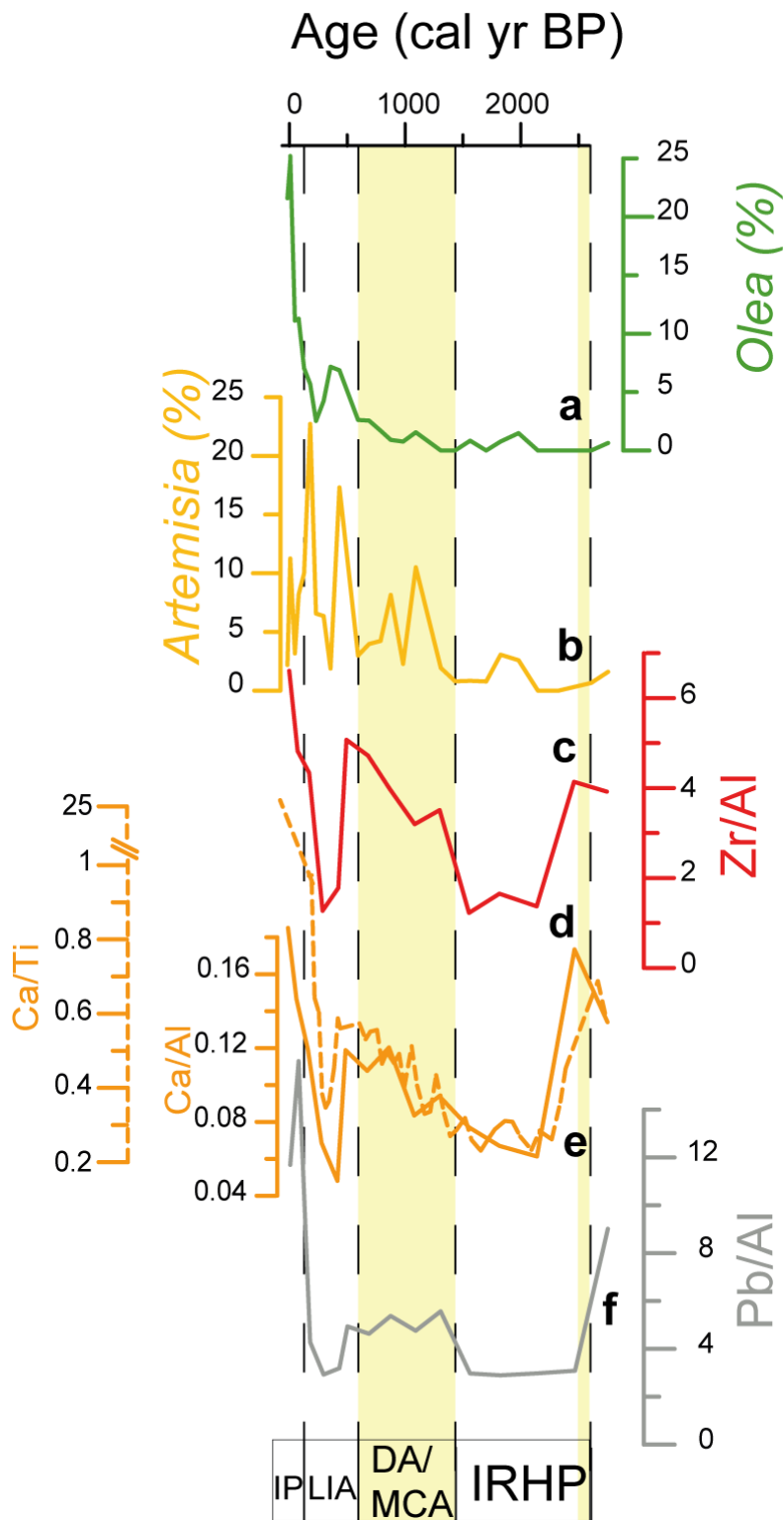
1072

1073

1074

1075

1076



1077

1078 **Figure 8.** Comparison of geochemical proxies with pollen taxa, related to anthropogenic impact for the last  
 1079 ~2600 cal yr BP. (a) *Olea* percentage from LH; (b) *Artemisia* percentage from LH record; (c) Zr/Al ratio  
 1080 from LH; (d) Ca/Al ratio from LH; (e) Ca/Ti (XRF) ratio from LH; (f) Pb/Al ratio from LH. Yellow bands  
 1081 indicate more arid intervals. Dark dashed lines are used for separating the different Current Era periods:  
 1082 IRHP: Iberian Roman Humid Period; DA: Dark Ages; MCA: Medieval Climate Anomaly; LIA: Little Ice  
 1083 Age; IP: Industrial Period.